Global Biogeochemical Cycles

RESEARCH ARTICLE
10.1029/2024GB008416

Physical Processes Driving Carbon Subduction in the Southern Ocean in an Eddy-Permitting Model

Simone Le Chevère[1,2], **Carolina O. Dufour**[1,3], **Laurent Bopp**[4], **and Marina Lévy**[5]

[1]Department of Atmospheric and Oceanic Sciences, McGill University, Montreal, QC, Canada, [2]Alfred Wegener Institute, Helmholtz Centre for Polar and Marine Research, Bremerhaven, Germany, [3]University Brest, CNRS, IRD, Ifremer, Laboratoire d'Océanographie Physique et Spatiale (LOPS), IUEM, Brest, France, [4]Laboratoire de Météorologie Dynamique (IPSL), Paris, France, [5]Laboratoire d'Océanographie et du Climat: Expérimentations et Approches Numériques (IPSL), Paris, France

Abstract The Southern Ocean south of 35°S represents a small source of natural inorganic carbon for the atmosphere but a major sink of anthropogenic carbon. The magnitude of the inorganic carbon sink, and the sequestration of inorganic and organic carbon strongly depend on the rate at which they are subducted below the mixed layer. We use a global ocean model at 0.25° resolution to quantify the drivers of the pathways of total and anthropogenic dissolved inorganic carbon (DIC) and organic carbon (OC) across and within the time-varying mixed layer of five physically consistent regions of the Southern Ocean over the period 1995–2014. Total DIC is brought into the mixed layer through obduction south of the Antarctic Circumpolar Current (ACC) and subducted north of the ACC, resulting in a net obduction of 11.2 PgC/year, with advective processes being responsible for about two-thirds of the total transfer. Anthropogenic carbon is brought to the mixed layer through the ocean surface in all regions but mainly subducted north of the ACC, with the subduction (1.05 PgC/year) being achieved through both advection and diffusion, each dominating respectively north and south of the Subantarctic Front. Two thirds of the organic carbon are subducted through the gravitational pump (1.9 PgC/year) and one-third through physical transfer (0.9 PgC/year), with an equivalent contribution from advection and diffusion. At the local scale, advective fluxes largely dominate other physical processes in transferring carbon across the base of the mixed layer, and are found to be increased near topographic features and boundary currents.

Key Points:

- We compute the inorganic and organic carbon fluxes within the mixed layer of five regions of the Southern Ocean in an eddying ocean model
- Advection dominates total carbon mixed layer base transfer but vertical diffusion contributes equally for anthropogenic and organic carbon
- Physical transfer, through advection and vertical diffusion, represents one third of the biological pump, its role decreasing with latitude

Supporting Information:

Supporting Information may be found in the online version of this article.

Correspondence to:

S. Le Chevère,
simone.lechevere@awi.de

Citation:

Le Chevère, S., Dufour, C. O., Bopp, L., & Lévy, M. (2026). Physical processes driving carbon subduction in the Southern Ocean in an eddy-permitting model. *Global Biogeochemical Cycles*, *40*, e2024GB008416. https://doi.org/10.1029/2024GB008416

Received 11 NOV 2024
Accepted 22 DEC 2025

Author Contributions:

Conceptualization: Laurent Bopp, Marina Lévy
Formal analysis: Simone Le Chevère
Funding acquisition: Carolina O. Dufour
Investigation: Simone Le Chevère, Carolina O. Dufour, Laurent Bopp, Marina Lévy
Methodology: Simone Le Chevère, Carolina O. Dufour, Laurent Bopp, Marina Lévy
Project administration: Carolina O. Dufour
Resources: Carolina O. Dufour, Laurent Bopp, Marina Lévy
Software: Simone Le Chevère
Supervision: Carolina O. Dufour, Laurent Bopp, Marina Lévy

1. Introduction

The Southern Ocean plays a dominant role in the global carbon cycle, as it is thought to be both a source of natural carbon dioxide (CO_2) to the atmosphere in winter and a major sink of anthropogenic carbon, accounting for up to 40% of the global ocean anthropogenic carbon sink (DeVries, 2014; Frölicher et al., 2015; Gruber et al., 2019; Sabine, 2004). This unique role of the Southern Ocean in the global ocean carbon cycle is mainly achieved thanks to its role as the primary ventilation region for deep waters in the global overturning circulation (Lumpkin & Speer, 2007; Marshall & Speer, 2012). Within and south of the Antarctic Circumpolar Current (ACC), the upwelling of the Circumpolar Deep waters (CDW) leads to significant carbon outgassing in the winter as these waters are rich in natural dissolved inorganic carbon (DIC) accumulated through remineralization (Gray et al., 2018; Mikaloff Fletcher et al., 2007; Talley, 2013). In contrast, CDW are poor in anthropogenic carbon due to the lack of exposure to the contemporary atmosphere (Graven et al., 2012; Orr et al., 2001). As a result, CDW absorb large amounts of anthropogenic carbon where they upwell (Mikaloff Fletcher et al., 2006; Sarmiento et al., 1992; Toyama et al., 2017). Part of the upwelled waters then head further south, where they contribute to the formation of denser waters within the Antarctic margins. The other part of the upwelled waters heads toward the North and transform into Antarctic Intermediate Water (AAIW) and Subantarctic Mode Waters (SAMW) to eventually subduct below Subtropical Waters, bringing with them the carbon absorbed along the way (Gruber et al., 2019). On average, the Southern Ocean is estimated to be a carbon sink at all latitudes, the absorption of anthropogenic carbon dominating over the outgassing of natural carbon (Gruber et al., 2019; Hauck, Gregor, et al., 2023).

The efficiency of the Southern Ocean carbon sink is ultimately limited by the carbon subduction rate, that is, the rate at which carbon is transferred from the mixed layer to the ocean interior (Bopp et al., 2015; Carroll et al., 2022; Davila et al., 2022; Iudicone et al., 2011; Levy et al., 2013; Sarmiento et al., 1992). Once atmospheric

Validation: Simone Le Chevère
Visualization: Simone Le Chevère
Writing – original draft: Simone Le Chevère
Writing – review & editing: Carolina O. Dufour, Laurent Bopp, Marina Lévy

CO_2 is taken up by the ocean, it is stored in the mixed layer in the form of DIC, where it partly remains subject to air-sea gas exchange. In the euphotic zone, DIC can also be used by autotrophic or mixotrophic organisms, and thereby transformed into dissolved and particulate organic carbon (DOC and POC, respectively) and carbon mass contained inside zooplankton and phytoplankton organisms, or be used by organisms to produce calcareous shells (called here particulate inorganic carbon, PIC; Boyd et al., 2019). For the sake of the discussion, we regroup all these terms of biologically induced carbon (with the exception of PIC which accounts for very little in terms of mass fluxes compared to POC and DOC in our model) under the global term of total organic carbon (TOC). TOC can also be transformed again into DIC through biological processes such as respiration and remineralization.

To be sequestered over long time scales that could reach decades to centuries, DIC and TOC need to be transferred (as well as to sink in the case of TOC) below the mixed layer base (Graven et al., 2012; Huang et al., 2023). The Southern Ocean is known to be a region with a particularly large injection of both total (natural + anthropogenic; Carroll et al., 2022; Levy et al., 2013) and anthropogenic carbon, representing more than 30% of the global injection of anthropogenic carbon to the ocean interior, thanks to the formation of intermediate waters (Bopp et al., 2015; Davila et al., 2022). This region is also estimated to represent around a third of the global export flux of POC (Schlitzer, 2002). Once subducted, anthropogenic carbon either remains below the mixed layer or is obducted, meaning that it is transferred from the interior back to the mixed layer. The reemergence of carbon within the mixed layer may occur only a few years after subduction in regions where processes support the upward transfer of carbon-rich waters, such as frontal and boundary current regions (Sallée et al., 2012; Toyama et al., 2017). The subduction and obduction of DIC through the mixed layer is called the solubility pump. The transfer of TOC below and back into the mixed layer is called the biological pump (Levy et al., 2013).

Inorganic and organic carbon subduction rates depend on several physical processes whose contribution may oppose in some regions and over some time periods. These processes include vertical advection (mostly driven by Ekman pumping and suction), horizontal advection across the sloped mixed layer base (sometimes referred to as lateral induction), along-isopycnal stirring and diffusion induced by mesoscale eddies and smaller scale features, vertical diffusion due to turbulent mixing across the mixed layer base, and seasonal entrainment/detrainment due to fluctuations of the mixed layer with seasons (see Figure 1b of Levy et al. (2013); see also Bopp et al. (2015), Boyd et al. (2019)). These processes do not have the same magnitude and role for natural DIC, anthropogenic DIC (hence for total DIC), and for TOC. Using a 2° global ocean model, Levy et al. (2013) find that vertical advection dominates the transfer of natural DIC across the mixed layer base in the Southern Ocean, leading to a net obduction, while obduction by vertical mixing is found to be one order of magnitude smaller. The authors also find that horizontal advection drives only a small part of natural DIC subduction and is partly countered by eddy mixing. In contrast, Dufour et al. (2013) find that vertical diffusion dominates over vertical advection for the obduction of natural DIC south of the Polar Front in a regional 0.5° ocean model. The physical transfer of anthropogenic DIC is found to be dominated by vertical mixing (mainly vertical diffusion) in ocean models (Bopp et al., 2015; Toyama et al., 2017). However, observation-based estimates of anthropogenic carbon subduction suggest that the role of vertical diffusion is negligible in regards to that of advection (Sallée et al., 2012). When looking at total DIC, Carroll et al. (2022) show that both advective and diffusive processes are important in subducting DIC across 100 m depth. In a recent observational study using BGC-Argo float measurements, Sauvé et al. (2023) found that advection dominates over mixing in bringing total DIC within the mixed layer south of the ACC and within the sea ice covered region. Therefore, the relative roles of advection and vertical mixing in the transfer of inorganic carbon across the mixed layer remain unclear.

Organic carbon (OC) is thought to be transferred primarily via biological transfer (i.e., the gravitational pump (Boyd et al., 2019; Levy et al., 2013)). However, other mechanisms need to be taken into account to obtain a realistic organic carbon export rate to depth, such as the physical transfer or the migrant pump (e.g., the vertical migration of organisms; Boyd et al., 2019; Dall'Olmo et al., 2016; Lacour et al., 2023; Nowicki et al., 2022; D. A. Siegel et al., 2023)). These other mechanisms were previously not accounted for in observation-based studies (e.g., Giering et al., 2023) despite the fact that physical transfer was shown to be important and maximized in regions of high productivity (Stukel & Ducklow, 2017). In fact, in the non-eddy-permitting model of Levy et al. (2013), the physical transfer of TOC below the mixed layer was shown to account for more than half of the gravitational pump and mainly driven by vertical mixing, due to the strong gradient of organic carbon at the base of the mixed layer and seasonal entrainment below the mixed layer in winter. Similarly, Boyd et al. (2019) suggest a total contribution of 40% of pumps other than the gravitational pump to the transfer of TOC to the ocean interior.

While the deployment of hundreds of autonomous biogeochemical Argo floats (BGC-Argo) since the 2010s has improved the quantification of air-sea CO_2 fluxes in all seasons (Gray et al., 2018; Sauvé et al., 2023; Williams et al., 2017), carbon subduction rates and their driving processes remain difficult to quantify from observations. Estimates of mixing notably depend on the poorly constrained eddy diffusivity coefficient, which is often estimated as constant over a large region, while diffusivity coefficients can vary by several orders of magnitude (Sauvé et al., 2023). Besides, the vastness of the Southern Ocean precludes any detailed spatial description of the carbon fluxes across the mixed layer, constraining observation-based estimates to be presented as quantities integrated over large regions.

Carbon subduction does not, however, occur at the same rate across the Southern Ocean. Regions of water mass formation within and north of the ACC are known to be particularly effective at subducting carbon (Davila et al., 2022; Mikaloff Fletcher et al., 2006). Within these regions, observations suggest localized sites of subduction and obduction (reemergence) of anthropogenic carbon located next to each other, in particular where the mixed layer is sloped with respect to the mean flow (Sallée et al., 2012). Away from the Antarctic shelves, ventilation of water masses have been shown to appear primarily along the ACC fronts and in limited regions such as the Drake Passage (Styles et al., 2024). This heterogeneous spatial distribution in the rates of transfer of natural and anthropogenic carbon across the mixed layer, that is, driven by lateral advective fluxes also clearly appears in numerical models (Bopp et al., 2015; Levy et al., 2013). Similarly, strong localized fluxes of organic carbon have also been reported in both observational studies (Accardo et al., 2025) and models (Resplandy et al., 2019). These fluxes are hard to quantify within large regions with sparse observations but may represent a large part of the biological carbon pump. In contrast, when driven through diffusion, fluxes of carbon generally show a more homogeneous distribution across the Southern Ocean with the exception of western boundary currents where enhanced fluxes are found (Bopp et al., 2015; Carroll et al., 2022; Dall'Olmo et al., 2016; Levy et al., 2013).

In this study, we identify and quantify the physical drivers of the transfer of inorganic and organic carbon across the mixed layer of the Southern Ocean within the recent decades of the historical period. Using a global eddy-permitting ocean model, we run twin experiments that only differ by the concentration of CO_2 in the atmosphere and of carbon in the ocean, thus allowing us to separate the anthropogenic from the natural component of the total inorganic carbon under historical conditions. Compared to prior work, the eddy-permitting resolution of our model allows for an improved representation of physical processes that transfer carbon across the mixed layer, and hence for a better understanding of how the carbon budget builds. The enhanced representation of scales and interactions with topography resulting from an increased resolution are all the more important at higher latitudes and in energetic and topographically constrained regions such as the Southern Ocean.

The rest of the paper is composed as follows. In Section 2, we investigate the performance of our model in representing the air-sea fluxes, the mixed layer and the stratification. In Section 3, we compute the budget of total and anthropogenic inorganic carbon, and of particulate and dissolved organic carbon within the mixed layer of five physically consistent regions of the Southern Ocean. Online diagnostics of carbon fluxes across the instantly varying mixed layer are performed to provide an exact decomposition of the physical drivers of the inorganic and organic carbon fluxes, and of the spatial patterns of carbon transfer. Finally Section 4 provides a discussion of our results and Section 5 summarizes the main results of the paper.

2. Methods

2.1. Model and Simulations

2.1.1. The eORCA025-PISCES Global Configuration

We use the NEMO (Nucleus for European Modeling of the Ocean) model platform, which comprises the ocean general circulation model OPA ("Océan Parallélisé") developed by Madec et al. (1998). OPA is coupled with the thermodynamical and dynamical Louvain-la-Neuve sea Ice Model (LIM3) which features five ice categories, each divided into one layer of snow and five layers of ice (Vancoppenolle et al., 2009). The ocean model includes the biogeochemical component Pelagic Interaction Scheme for Carbon and Ecosystem Studies (PISCES; Aumont et al., 2015) which holds 24 prognostic tracers. PISCES includes two phytoplankton functional types (diatoms and nanophytoplankton), two zooplankton size-classes (micro- and mesozooplankton), and five nutrients which are phosphate (PO_4), ammonium (NH_4), nitrate (NO_3), silicium (Si) and iron (Fe). In addition, PISCES includes four prognostic carbon variables: DIC, dissolved organic carbon (DOC), particulate organic carbon (POC) and

particulate inorganic carbon (PIC), as well as alkalinity. The DIC concentration is partitioned into three species ($DIC = HCO^{-}_{3(aq)} + CO^{2-}_{3(aq)} + CO_{2(aq)}$) following the Ocean Carbon-Cycle Model Intercomparison Project protocols (Orr et al., 2017).

We have two main caveats in our experimental design. First, we do not take into account the migrant pump (i.e., the transport of carbon through the vertical migration of marine organisms), as we do not diagnose it with our model. However it has recently shown to have an increasingly important role for the biological pump in the Southern Ocean, being on the same order of magnitude as the physical transfer (Archibald et al., 2019; Baker et al., 2025; Nowicki et al., 2022). Second, in our results, we only represent the fluxes of labile or semi-labile DOC, as the refractory DOC is a set value constant at the surface. Refractory DOC has a very long lifespan and is not consumed or created during the studied period. However, not taking into account the refractory DOC could entail that the advective fluxes DOC are smaller compared to observational values (Hansell, 2013; Resplandy et al., 2019).

CO_2 sea-air fluxes are computed following Wanninkhof (1992):

$$F_{CO_2} = \left(1 - f_{ice}\right) \times K\left(pCO_2^{ocean} - pCO_2^{atm}\right) \quad (1)$$

with K the gas transfer velocity depending mainly on the temperature and the wind speed, the partial pressure of CO_2 in the ocean (pCO_2^{ocean}) and in the atmosphere (pCO_2^{atm}), and f_{ice} the sea ice total fraction. All results are presented averaged over the period 1995–2014 (the last 20 years of our simulations). The eORCA025 global configuration is used to run the model (Madec & the NEMO Team, 2016). This configuration has a tripolar grid with a global orthogonal curvilinear ocean mesh applied to a Mercator projection. The nominal horizontal resolution is 0.25° resulting in grid sizes of around 17 km at 50°S and 5.6 km (zonal direction) and 3.2 km (meridional direction) at the highest latitudes (Madec & the NEMO Team, 2016). Antarctic under-ice shelf seas are represented to account for the contribution of the ice-shelf–ocean interactions to the Southern Ocean freshwater cycle (Mathiot et al., 2017). In the vertical, the water column is split in 75 levels with grid thickness increasing from 1 m at the surface to around 200 m at the bottom. The 0.25° resolution only allows for the partial resolution of mesoscale eddies in the Southern Ocean (Hallberg, 2013). Hence, the parameterizations of Gent and McWilliams (1990) and Redi (1982) are used with small coefficients of 300 $m^2\ s^{-1}$ and 100 $m^2\ s^{-1}$, respectively, to obtain physical and biogeochemical fields that remain close to observations while maintaining an explicit representation of oceanic mesoscale features. In coarser resolution configurations, those coefficients are typically set to much larger values: for example, both coefficients are set to 2000 $m^2\ s^{-1}$ in ORCA_R2, the 2° resolution counterpart of ORCA025 (Bopp et al., 2015).

2.1.2. The Twin Simulations

Two simulations are run with the eORCA025-PISCES configuration: one with preindustrial atmospheric CO_2 conditions simulating the carbon naturally present in the ocean (NAT), and one with historical CO_2 conditions simulating the total carbon which includes the anthropogenic component (TOT), following the modeling protocol of the models and observational products consortium Global Carbon Budget (GCB; Hauck et al., 2020). In NAT, an atmospheric CO_2 concentration of 278 ppm, corresponding to the year 1850, is kept constant throughout the simulation. Anthropogenic carbon emissions from 1765 to 1850 are thus not accounted for. NAT is initialized from GLODAPv2 preindustrial DIC field (Olsen et al., 2016). In TOT, the atmospheric CO_2 concentration follows the GCB time series (Friedlingstein et al., 2020). TOT is initialized in 1958 with GLODAPv2 total DIC concentrations computed by adding to the preindustrial DIC field the anthropogenic DIC field from year 1958 of the ORCA05 simulation used to initialize the simulations run in Terhaar et al. (2019). Both simulations are directly run without further spin up from 1958 to 2014 using the atmospheric fields from the Drakkar forcing set 5 version 2 (DFS5; Dussin et al., 2016), which has been designed explicitly for running ocean-only simulations until 2014. Both TOT and NAT are thus run under the same historical conditions, so they share the same circulation and physical ocean properties. In addition, biological processes are unchanged between TOT and NAT since it is assumed that these processes are not impacted by the addition of anthropogenic carbon given that dissolved inorganic carbon is not a limiting factor. Subtracting NAT from TOT enables to obtain the anthropogenic component of carbon in the ocean over the period studied and to follow its penetration into the ocean interior which has been shown to be the predominant source of carbon content increase in the Southern Ocean

(Hauck, Gregor, et al. (2023), their Figure 3). Thus, the anthropogenic carbon is not an actual tracer, the advection and diffusion of anthropogenic carbon being estimated from that of total and natural carbon.

2.2. Observational Products

To evaluate the modeled sea-air CO_2 fluxes, we use the observation-based product of Bushinsky et al. (2019). This product uses a neural network method to reconstruct pCO_2 during the period 2015–2017 by combining the pCO_2 climatology of the Surface Ocean CO_2 Atlas (SOCAT; Landschützer et al., 2020) from 1982 to 2017 and the SOCCOM data set from Gray et al. (2018). The SOCCOM data set is built on Argo-float data collected between 2014 and 2017 (Bushinsky et al., 2019). We also use the CO_2 flux climatology from the Global Carbon Budget (Hauck et al., 2020). Mixed layer observations are provided by a climatology that includes Argo floats profiles taken from 2001 to 2015 (Hosoda et al., 2010).

2.3. Analyses

2.3.1. Southern Ocean Regions

To compare the modeled sea-air CO_2 fluxes to observational estimates, we use the five Southern Ocean regions defined in Gray et al. (2018) for all of our analyses. Each region corresponds to a different dynamical and biogeochemical province of the Southern Ocean south of 35°S and each boundary is averaged over the 20-year period of 1995–2014. The boundaries of the regions are defined using the dynamical and biogeochemical characteristics of our model to ensure consistency with the model solution. The five regions are defined as follows (see also Figure 1):

- *The Sea Ice Zone (SIZ)* is defined as the region where the September sea ice concentration is greater than 15% and is bounded at the north by the Sea Ice Front. This region which is where the Circumpolar Deep Water upwell and the Antarctic Bottom Water form, has a strong seasonality due to the sea ice cover.
- *The Antarctic Southern Zone (ASZ)* is located between the Sea Ice Front and the Polar Front, these two fronts defining a wind-driven divergence area forcing the upwelling of Circumpolar Deep Waters. The Polar Front location is defined using a sea surface height (SSH) contour identified at a local maximum of SSH meridional gradient. This local maximum is searched for within a [−0.5°; +2°] band around the northernmost location of the 2°C isotherm between 50 and 300 m. This latter location is used to track the equatorward penetration of the Antarctic Winter Waters (Park et al., 1998). The SSH contour selected to define the location of the Polar Front is computed as the average of 10 SSH contours each defined at different longitudinal sections across the Southern Ocean following Dufour et al. (2015).
- *The Polar Frontal Zone (PFZ)* is located between the Polar Front and the Subantartic Front, and corresponds to the zone of formation of Antarctic Intermediate Waters which head northward from there. The Subantarctic Front location is defined using a SSH contour identified at a local maximum of SSH meridional gradient. This local maximum is searched for within a latitudinal band varying from 1° to 10° (depending on the longitudinal section) south of the winter mixed layer depth (MLD) maximum found north of the ACC. This maximum identifies the region of formation of Subantarctic Mode Waters (Li et al., 2021; Orsi et al., 1995). The SSH contour of the Subantarctic Front is computed as the average of 8 SSH contours each defined at different longitudinal sections across the Southern Ocean, similarly to the PF (but excluding two locations where the Subantarctic Front is not clearly distinct).
- *The Subantarctic Zone (SAZ)* is located north of the Subantarctic Front and south of the Subtropical Front, and is a convergence zone where Subantarctic Mode Waters are formed. The Subtropical Front corresponds to the location of the 11°C isotherm of conservative temperature at 100 m following Orsi et al. (1995).
- *The Subtropical Zone (STZ)*, where warm Subtropical Waters driven by western boundary currents heading poleward are found, is defined north of the Subtropical Front and south of 35°S, the northernmost extent of our domain.

When comparing the areas of our regions to that of Gray et al. (2018), we find mismatches of the order of 5%–18% (Table 1). These mismatches arise from biases in the modeled circulation, hydrography and sea ice, but also from slight differences in front definitions with Gray et al. (2018) and from the inclusion of ocean areas shallower than 1,000 m (coastal areas) in our study in contrast to that of Gray et al. (2018). The inclusion of coastal areas in our study yields a difference of $-1.2\ 10^5$ km^2 below 60°S and of $+0.33\ 10^7$ km^2 between 35°S and 60°S with the areas of Gray et al. (2018). The area of ocean below 60°S is smaller in our model than in the observational

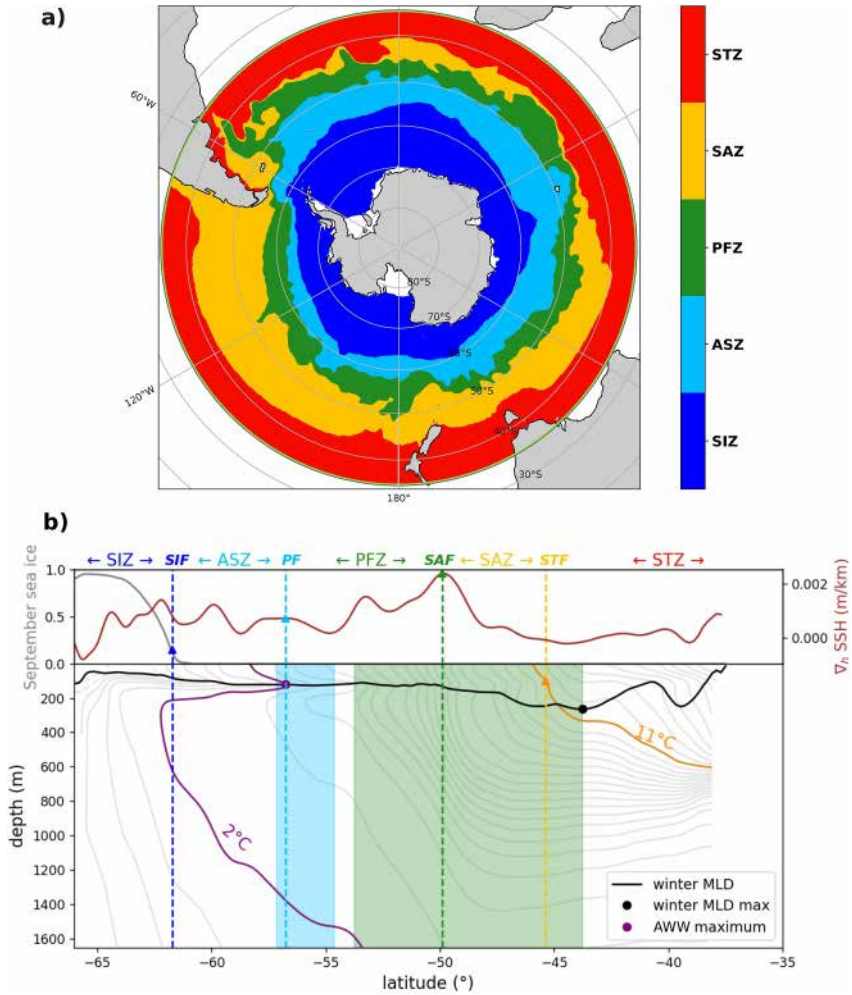

Figure 1. (a) The five regions of the Southern Ocean used in the study. From South to North: Sea Ice Zone (SIZ), Antarctic Southern Zone (ASZ), Polar Frontal Zone (PFZ), Subantarctic Zone (SAZ), and Subtropical Zone (STZ). (b) Example of the boundary detection procedure for 140°E, one of the meridional sections used to define the Polar Front and Subantarctic Front. The Sea Ice Front, Polar Front, Subantarctic Front and Subtropical Front are represented in dotted lines. In the top panel, the September sea ice fraction is represented in gray, with the triangle at 0.15 marking where we define the Sea Ice Front. The potential temperature is contoured in the background of the bottom panel with the 2°C isotherm highlighted in purple along with the northernmost extent (purple dot) corresponding to the Antarctic Winter Waters (AWW). The [−0.5°, 2°] band (blue shading) is the region where a local maximum in the SSH meridional gradient (brown curve in the top panel) is searched for. The location of this maximum defines the location of the Polar Front (light blue triangle). Note that in this example the purple dot and light blue triangles align, but that is not necessarily the case for every section investigated. The winter MLD (black curve; bottom panel) shows a maximum north of the ACC. A 10° latitudinal band south of this maximum (green shading) is defined to search for the local maximum of the SSH meridional gradient corresponding to the location of the Subantarctic Front (green triangle; top panel). Finally, the latitude where the 11°C isotherm (orange curve) crosses the 100 m isobath (orange triangle) defines the location of the Subtropical Front.

products used by Gray et al. (2018), though by a very small amount, because of a higher resolution of the Antarctic coastlines in the model. For the SIZ, which is delimited by the continent south of 60°S, the difference in area between our study and that of Gray et al. (2018) is thus negligible (less than 1% of the SIZ area). However, for the STZ and SAZ, in which most of the coastal area north of 60°S is located, the difference is not negligible as it accounts for about 8% of the total areas of theses regions. While these differences impact in turn the comparison of air-sea CO_2 fluxes integrated over regions between our study and observations, they remain of secondary importance in front of differences arising from model representation of the physics and biogeochemistry of the Southern Ocean.

Table 1
Areas of the Five Regions of the Southern Ocean (in 10^7 km^2) in the eORCA025 Model and in Observations (Gray et al., 2018), and Relative Differences Between the Model and Observations

	SIZ	ASZ	PFZ	SAZ	STZ	Total
eORCA025	2.03	1.47	1.25	2.04	2.48	9.27
Gray et al. (2018)	1.72	1.28	1.43	1.94	2.26	8.64
Rel. error (%)	18	15	−13	5	10	7

Note. Definitions are detailed in Section 2.3.1 and the regions are represented in Figure 1.

2.3.2. Carbon Budgets in the Mixed Layer

Within a given region, budgets of natural and total DIC in the mixed layer are computed offline from this equation:

$$\frac{\partial C}{\partial t} - F_{C,sea-air} + F_{C,sub} - \nabla_h F_{C,bound} - F_{C,i/o} + Res_i = 0 \quad (2)$$

with $\partial C/\partial t$ the tendency of tracer C (here the DIC) in the mixed layer, $F_{C,sea-air}$ the CO_2 sea-air fluxes, $F_{C,sub}$ the physical transfer of carbon across the base of the mixed layer, $\nabla_h F_{C,bound}$ the horizontal divergence of DIC fluxes across the fronts, and $F_{C,i/o}$, the term of transfer of inorganic carbon to organic carbon (through primary production, respiration and remineralization; see detailed explanation of its computation in Equations 3–5).

$\nabla_h F_{C,bound}$ is obtained from the computation of horizontal fluxes of carbon across the boundaries of the regions using monthly averaged horizontal velocities and tracer concentration for total DIC. Res_i is a residual term for total and natural DIC and is the sum of errors resulting from the offline computation of horizontal fluxes across the fronts, the horizontal diffusion (parameterized by the Redi diffusion scheme (Redi, 1982)) through the fronts, that is not accounted for here due to the lack of the necessary model output, as well as the river runoff. The river runoff amounts to an additional 0.013 PgC/yr of inorganic carbon south of 35°S, and is therefore a secondary term in the residual, dominated by the error in the horizontal fluxes (advection and diffusion). There are no errors in the subduction and air-sea CO_2 fluxes diagnostics, as they are computed directly online at each timestep of the model.

For the budget of anthropogenic DIC, each term is computed from the difference between the budget terms of the total and natural DIC (using Equation 2) except for the horizontal divergence which is computed as the residual term of the budget. In the case of anthropogenic DIC, the residual term only includes the horizontal divergence because there is no biological process nor river runoff, since these two terms are identical between the TOT and the NAT simulations. Defining the horizontal divergence as the residual thus allows us to remove the uncertainty linked with its computation based on monthly averaged fields.

Similarly, the budgets of DOC and POC within the mixed layer are computed from this general equation:

$$\frac{\partial C}{\partial t} + F_{C,sub} + Sinking_{POC} - \nabla_h F_{C,bound} + Res_o = 0 \quad (3)$$

The terms $\frac{\partial C}{\partial t}$, $F_{C,sub}$, $\nabla_h F_{C,bound}$ are computed in the same way as in Equation 2 for C representing the DOC or the POC. The gravitational pump $Sinking_{POC}$ describes the gravitational sinking of POC through the mixed layer base and is not a process affecting DOC in our model. Res_o is a residual term and is the sum of $F_{C,i/o}$ (Equation 2) as well as, similarly to inorganic carbon calculation, the error deriving from the offline computation of $\nabla_h F_{C,bound}$, and the horizontal diffusion of DOC and POC across the fronts.

In the model, the horizontal advection of both DOC and POC across the boundaries of the regions reaches at most one third of the magnitude of Res_o. Therefore, Res_o is not dominated by errors in the horizontal advection nor by horizontal diffusion (likely smaller than horizontal advection) but by the transfer from inorganic to organic carbon, $F_{C,i/o}$. We thus do the following approximation:

$$Res_o \sim F_{C,i/o} \quad (4)$$

We can therefore rewrite Equation 3 as follows:

$$\frac{\partial C}{\partial t} + F_{C,sub} + Sinking_{POC} - \nabla_h F_{C,bound} + F_{C,i/o} \sim 0 \quad (5)$$

$F_{C,i/o}$ is thus calculated as a residual term in Equation 5 and then passed on to Equation 2.

2.3.3. Computation of the Transfer of Carbon Across the Mixed Layer Base

The transfer of carbon across the base of the mixed layer is computed online at every time step of the model across the time-varying mixed layer base (also computed at each model time step) from the sum of several fluxes that we combine following Karleskind et al. (2011), Levy et al. (2013), and Bopp et al. (2015):

$$F_{C,sub} = \int_t \left(\underbrace{-C_h(w_h + \boldsymbol{u}_h \,.\, \nabla h) + F_{C,GM}}_{\text{total advection}} + \underbrace{k_z^h \partial_z C_h}_{\text{vertical diffusion}} \underbrace{-C_h \partial_t h}_{\substack{\text{seasonal} \\ \text{entrainment}}} + \underbrace{F_{C,Redi}}_{\substack{\text{Parameterized} \\ \text{isopycnal diffusion}}} \right) dt \quad (6)$$

The *total advection* term is the total (vertical and horizontal) advection of tracer C (here DIC,DOC or POC) through the base of the mixed layer, where C_h is the concentration of the tracer, w_h and $\mathbf{u}_h$ are respectively the vertical and horizontal velocity at the base of the mixed layer (subscript h), and $F_{C,GM}$ the subduction by the parameterized eddy driven transport (Gent et al., 1995). $F_{C,GM}$ represents only around 5% of the total advection term given that the coefficient used is relatively small (see Section 2.1). For this reason, we combine the parameterized and resolved advection term in our analysis. The *vertical diffusion* term corresponds to the vertical diffusion of tracer C across the mixed layer base, with k_z^h the vertical diffusion coefficient and $\partial_z C_h$ the vertical gradient of C across the base of the mixed layer. Vertical diffusion coefficients k_z^h are derived from the Turbulent Kinetic Energy (TKE) closure scheme of Blanke and Delecluse (1993) with improvements from Madec (2008) and vary around 1.2 10^{-5} m^2 s^{-1}. The *seasonal entrainment* term is the entrainment/detrainment of C due to the temporal variations of the MLD h. Finally, the *parameterized isopycnal diffusion* term, $F_{C,Redi}$, corresponds to the along-isopycnal diffusion of C at the mixed layer base (Redi, 1982). In the transfer of POC across the base of the mixed layer, the gravitational sink of particulate matter $Sinking_{POC}$, represented in our model by two different sinking speeds for small and larger particles, is taken into account as an additional term of transfer. Organic carbon fluxes are also often grouped within the advective pump, including the advection and isopycnal stirring and diffusion in our model, and the mixed-layer pump, including the vertical diffusion and the seasonal entrainment in our model. We will refer to these pumps in the discussion (Section 4).

2.4. Evaluation of the Simulations

2.4.1. Mixed Layer Depth and Stratification

In the model, the spatial distribution of the MLD is overall similar to that of the observations (Figures 2a–2e). In particular, deep MLD patterns in the East Pacific and Indian sectors are well represented, with a moderate downstream (eastward) shift of the deepest MLD compared to observations (Figures 2c and 2d). The deep MLD found in the model south of the South African coast in the STZ, however, does not appear in observations. We find that in both summer (January) and winter (August), the modeled MLD is on average shallower than the observed MLD by ∼10 m and ∼20 m, respectively, between 35°S and 70°S. The shallow summer bias likely comes from a lack of wind energy input in our model or from the vertical mixing parameterization scheme that does not account for some wind effects (e.g., swells, near-inertial oscillations; Rodgers et al., 2014). Deep bias is generally found in non-eddy-permitting and eddy-permitting models in winter due to the lack of restratification by mesoscale eddies. Refining the horizontal resolution and/or adding a mesoscale eddy transport parameterization both act in reducing this bias (Adcroft et al., 2019). Running our model with both parameterization and eddy-permitting resolution might be the reason for the absence of this bias.

The model generally reproduces a stratification similar to that observed (see Figures S1d–S1f in Supporting Information S1). We note, however, a high bias in salinity in the upper and subsurface ocean of the model that impacts the representation of AAIW. There is also a low bias in density at depth south of 60°S which is typical of z-coordinate models which are known to have a poor representation of the processes leading to the overflow and sinking of dense shelf waters along the Antarctic continental slope (Adcroft et al., 2019).

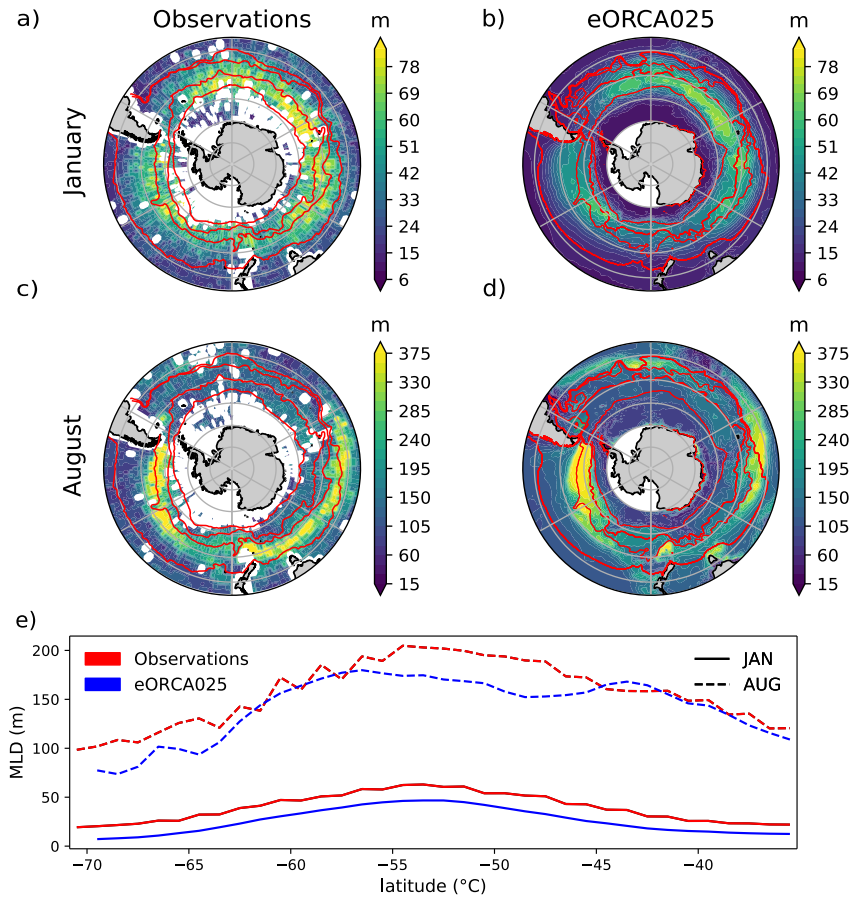

Figure 2. MLD for (a, b) January (month of the shallowest mixed layer) and (c, d) August (month of the deepest mixed layer) averaged over the period 1995–2014 (our model) and 2001–2015 (observations). This time period is the best overlap between the observational data set and simulation time periods. Observations (a, c) are from Hosoda et al. (2010) and are based on Argo floats measurements using the density criterion of $\Delta\sigma = 0.03$ kg m^{-3} following de Boyer Montégut (2004). The boundary of the five regions are represented with red contours using the observation-based boundaries from Gray et al. (2018) in panels (a, c) and the method described in Section 2.3.1 and applied to the model output in panels (b, d). Panel (e) shows the zonal average of MLD in our model and the observations for both January and August.

2.4.2. Sea-Air CO_2 Fluxes

Over 2009–2014, -1.13 ± 0.05 PgC/year of CO_2 is absorbed by the ocean south of 35°S in the model (Figure 3). CO_2 is taken up in all regions of the Southern Ocean, including south of the ACC, in accordance with observations from SOCAT, while SOCAT + SOCCOM combined data give an outgassing in the ASZ. When averaged over the Southern Ocean, the total uptake is found to be very similar to the SOCAT estimate, but it results from a compensation between a higher uptake south of and within the ACC (SIZ, ASZ, PFZ) and a lower uptake north of the ACC (SAZ, STZ). When compared to the SOCAT + SOCCOM data set, the model shows a higher uptake in all regions but the STZ. The SOCCOM data set shows an ougassing in the SIZ and ASZ, in contrast to the SOCAT data set and most biogeochemical ocean models: this disagreement was hypothesized to arise from the year-round sampling of BGC-Argo floats in this region or to biases in the float pH measurements (Bushinsky et al., 2019; Gray et al., 2018; Maurer et al., 2021). Finally, while the modeled sea-air fluxes evolve within the range of estimates provided by the Global Carbon Budget (GCB) over 1995–2014 below 35°S, they show an increase at a slightly faster rate (1.1 10^{-2} mol/m^2/year^2 when linearly fitted between 1965 and 2014) than the average of GCB models (9.8 10^{-3} mol/m^2/year^2), which indicates a stronger sink (Figure S2 in Supporting Information S1). These higher sink and higher sink rate can explain a higher surface total DIC concentration found at the surface in our model (Figure S4b in Supporting Information S1). A caveat on this analysis is that we use the time period 2009–2014, while the SOCCOM + SOCAT data and the SOCAT data span over the period 2015–2017

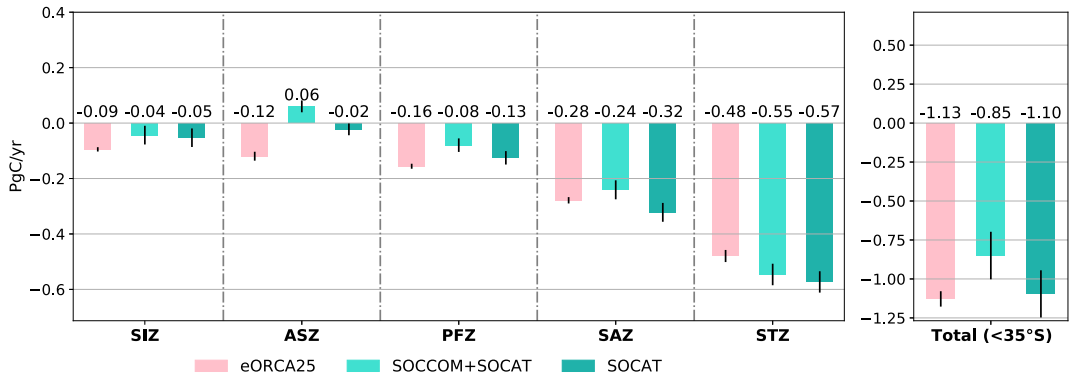

Figure 3. Sea-to-air CO_2 fluxes integrated over (left) each of the five regions defined in Section 2.3.1 and (right) the Southern Ocean (south of 35°S) in the TOT simulation (pink) and two observation-based products (green): the SOCAT data set (Bakker et al., 2016) and the combination of SOCCOM and SOCAT data sets by Bushinsky et al. (2019). Positive fluxes correspond to outgassing. Model fluxes are integrated between 2009 and 2014, while observations reflect measurements from 2015 to 2017 Bushinsky et al. (2019). Error bars correspond to interannual variability in the model, and combine the interannual variability and a method uncertainty of ±0.15 PgC in Bushinsky et al. (2019). Note that the vertical scale is different between the five regions (left) and the Southern Ocean (right).

(Bushinsky et al., 2019)). Given the decadal variability in CO_2 (Landschützer et al., 2016), comparing estimates spanning different time periods might be one of the main sources of disagreement between these different products. Indeed, from year 2009 to 2017, pCO_2 products show a positive trend in the uptake of 0.258 PgC/year/decade between 2001 and 2018 in observation-based products (RECCAP2 project, Hauck, Gregor et al. (2023)). Taking the observational estimate, we compute an increase of 0.08 PgC/year between 2009–2014 and 2015–2017 in our model. This 0.08 PgC/year would bring the model even further away from the observations.

3. Results

3.1. Fluxes of Total Dissolved Inorganic Carbon Within the Mixed Layer

3.1.1. Budget Within the Mixed Layer

Within the Southern Ocean mixed layer, fluxes of total DIC (DIC_{tot}) primarily originate from the transfer of DIC_{tot} across the mixed layer base and from the fluxes across the fronts separating the regions (Figure 4a). Across the base of the mixed layer, DIC_{tot} is transferred at a rate of 11.2 PgC/year (Figure 4b). This net rate results from compensating obduction and subduction, which dominate respectively south and north of the ACC in accordance with the overturning circulation. South of the Subantarctic Front, there is a large obduction of 21.6 PgC/year (Figure 4a) driven by the upwelling of Circumpolar Deep Waters. Once obducted in the mixed layer of the SIZ and of the ASZ, and to a lesser extent of the PFZ, or once taken up at the air-sea interface, DIC_{tot} is transported northward across all the fronts of the ACC (Figure 4a). This consistent northward transport implies that most of the DIC found in the mixed layer of the northernmost regions of the Southern Ocean is of Southern Ocean origin, which is consistent with the physical circulation and large-scale DIC gradients in the Southern Ocean (DeVries et al., 2017; Gruber et al., 2019). The STZ and SAZ, north of the Subantarctic Front, show a comparatively weaker subduction of 10.4 PgC/year (Figure 4a). These two regions see the subduction of Antarctic Intermediate Waters and Subantarctic Mode Waters below warmer Subtropical Waters. Almost half of the DIC_{tot} transported north of the Subantarctic Front within the mixed layer is subducted to the ocean interior within the Southern Ocean. The other half is transported north of 35°S (6.53 PgC/year), that is, out of the Southern Ocean, or is removed largely by biological processes north of the Subantarctic Front (1.9 PgC/year transferred to the increase rate in DOC and POC in the SAZ and the STZ - Figures 6a and 7a). Overall, although large amounts of DIC_{tot} are brought to the mixed layer by upwelled Circumpolar Deep Waters, only a small fraction is outgassed, while the bulk of it is transported northward and then largely subducted north of the ACC. Air-sea fluxes are generally at least an order of magnitude smaller compared to the DIC_{tot} transport terms within and at the base of the mixed layer, but provide a comparatively larger contribution in the northernmost regions due to enhanced fluxes in western boundary currents and in the subtropical Atlantic Ocean (Figure S3 in Supporting Information S1). We note that the sum of errors in estimating horizontal fluxes across region boundaries and river runoff (the residual term; see Section 2)

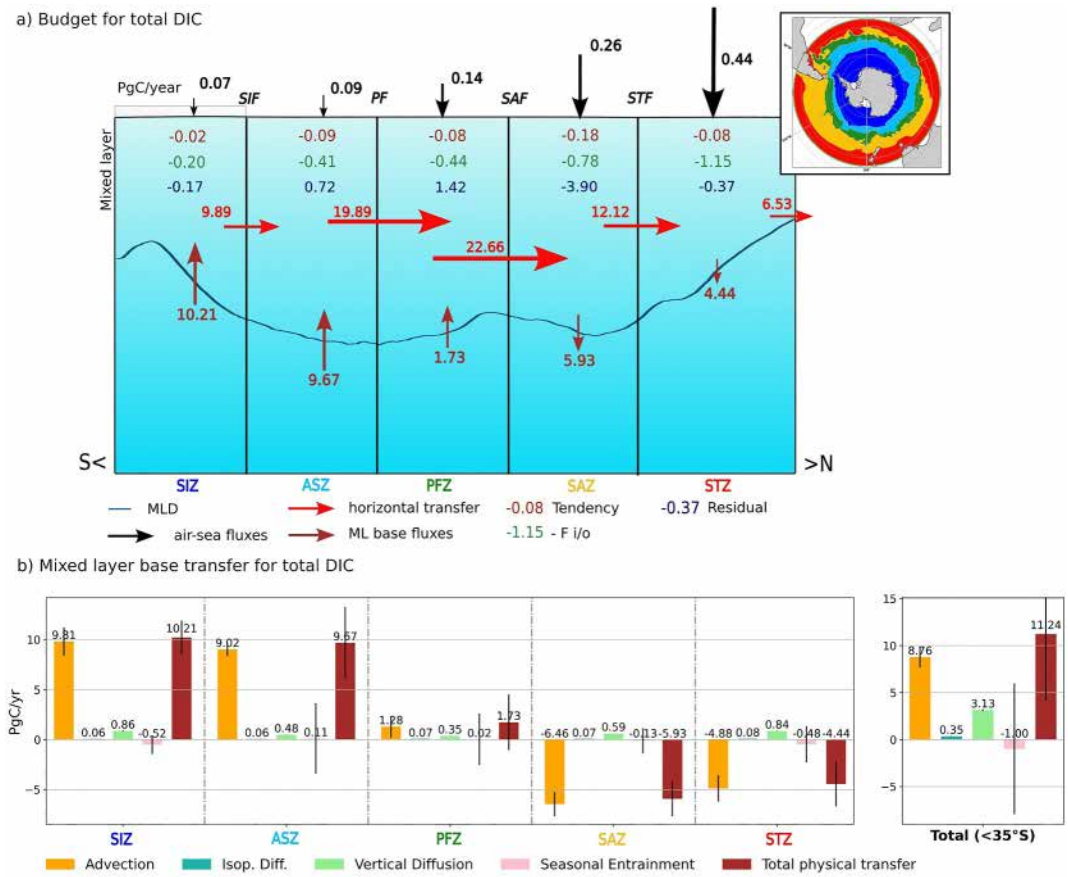

Figure 4. (a) Budget of total DIC in the mixed layer averaged over 1995–2014 for each of the five regions of the Southern Ocean (see definition in Section 2.3.1). The budget terms are computed following Equation 2 and expressed in PgC/year. The size of arrows used for horizontal and mixed layer fluxes is 1/40 compared to the scale used for air-sea fluxes. Positive values in the mixed layer indicate a gain of DIC. The insert indicates the five regions of the Southern Ocean as described in Figure 1a and Section 2.3.1. (b) Decomposition of subduction fluxes across the base of the mixed layer for each region into the different processes following Equation 6. Positive fluxes correspond to obduction of DIC within the mixed layer. Error bars correspond to the interannual variability over 1995–2014.

are of the same order of magnitude as the transfer of total DIC to organic carbon in all regions, in particular in the SAZ, possibly due to the energetic Subantarctic Front which bounds this region.

Over 1995–2014, no significant net accumulation nor loss of DIC_{tot} occurs in the mixed layer of the Southern Ocean (Figure S5a in Supporting Information S1), and no significant trend occurs either in any of the DIC fluxes within or across the mixed layer in any region of the Southern Ocean. This lack of long-term trend may result from the relatively short time period investigated and may be explained by a comparatively large decadal variability driven by oceanic and atmospheric forcings (Landschützer et al., 2016).

3.1.2. Physical Drivers of Total Carbon Transfer Across the Mixed Layer Base

In the model, the transport of DIC_{tot} across the base of the mixed layer is found to be dominated by advection which represents the major part (>80%) of obductive fluxes south of the Subantarctic Front, and of subductive fluxes north of the Subantarctic Front (Figure 4b). Therefore, advection appears to be the dominant driver of subduction in all regions, but due to compensation between obductive fluxes in the south and subductive fluxes in the north of the Subantarctic Front, it only represents 67% of the transfer of DIC across the base of the mixed layer in the Southern Ocean (Figure 4b). At the scale of the Southern Ocean, the other important contributor of the total physical transfer of DIC_{tot} across the mixed layer base is vertical diffusion which contributes at 23%. Although about an order of magnitude smaller than the advective term within each region (Figure 4b), the vertical diffusive term consistently brings carbon into the mixed layer of all regions (as DIC_{tot} increases with depth), providing an

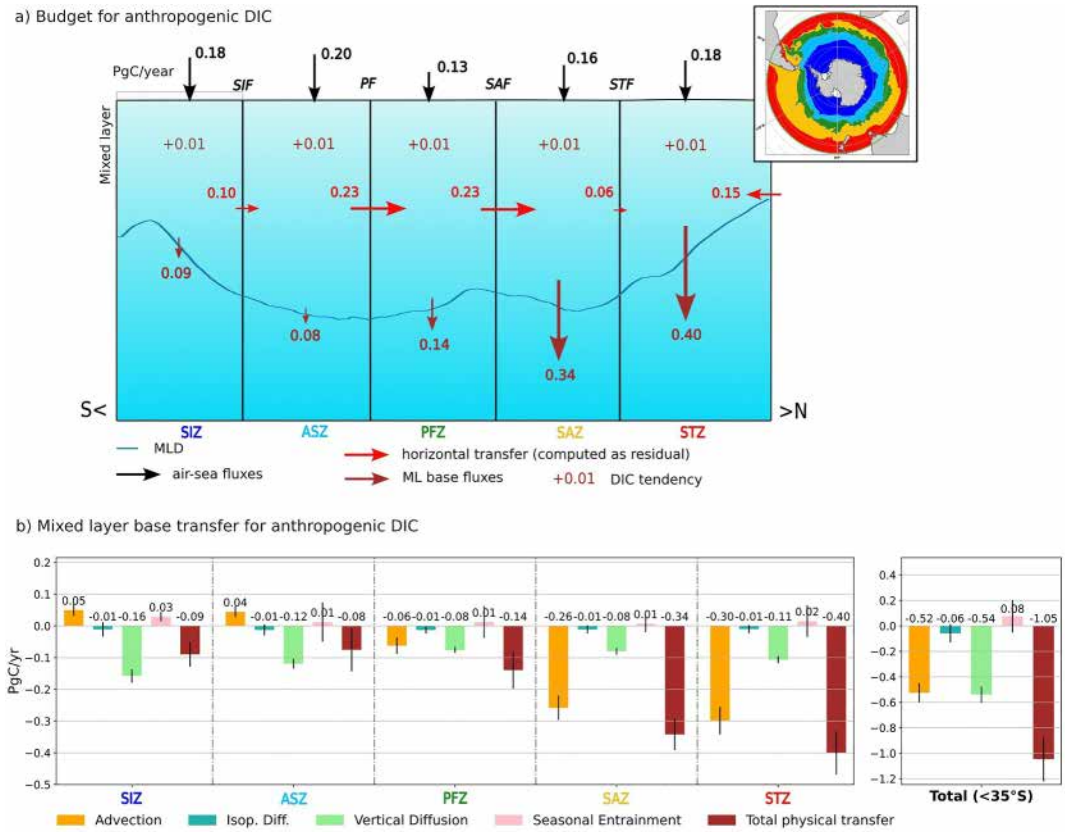

Figure 5. Same as Figure 4 but for DIC_{ant} except for air-sea fluxes which use the same scale as the other fluxes here.

important pathway for carbon to the mixed layer at the scale of the Southern Ocean. The contribution of this term is greatest in the SIZ and the STZ where vertical mixing can be enhanced by strong gradients across the base of the mixed layer (SIZ; see Figures S4a and S4b in Supporting Information S1) or intensified turbulent mixing in western boundary currents (STZ). The remaining fluxes of DIC_{tot} across the mixed layer base, seasonal entrainment and isopycnal diffusion, account for a very small fraction of the transfer within all regions, amounting to only 10% of the transfer over the Southern Ocean. Of the two terms, isopycnal diffusion is the smallest and is mostly driven by its vertical component (not shown). The seasonal entrainment term, while generally several times bigger than the isopycnal diffusion term, has a relatively small contribution over the period due to a large interannual variability showing positive and negative contributions compensating over the years (Figure 4b).

3.2. Fluxes of Anthropogenic Dissolved Inorganic Carbon Within the Mixed Layer

3.2.1. Budget Within the Mixed Layer

Air-sea fluxes are the primary source of DIC_{anth} in the mixed layer with an uptake at the surface that ranges from 0.13 PgC/year to 0.18 PgC/year across the five regions (Figure 5a). This small range between regions arises in part from compensation between the magnitude of fluxes within a region and its size. In particular, while the ASZ is the smallest of the five regions, it shows the largest fluxes (see Table S1 in Supporting Information S1), due to the upwelling of old Circumpolar Deep Waters in this region (Figure 4c).

Within the Southern Ocean mixed layer, the primary sink of DIC_{anth} is its subduction toward the ocean interior which amounts to 1.05 PgC/year (Figure 5b, total fluxes). The DIC_{anth} uptaken at the surface of the Southern Ocean represents 81% of the subducted DIC_{anth}, the remaining 19% being brought from the subtropical regions north of 35°S (14%) or from carbon already stored in the mixed layer (5%). Seventy-one percent of the subduction of DIC_{ant} in the Southern Ocean occurs in the northernmost regions (SAZ and STZ), explaining the deep penetration of the anthropogenic signal seen in these regions (Figure S4c in Supporting Information S1). This

penetration is associated with the subduction of water masses, primarily of the Subantarctic Mode Waters. In contrast, the SIZ, the ASZ and to a lesser extent the PFZ, show subduction rates around four times smaller than that of the northernmost regions.

Our analyses show that DIC_{anth} is transported northward into the SIZ, ASZ and PFZ most likely by the Ekman transport, while a southward transport, probably associated with western boundary currents brings DIC_{anth} from the subtropical regions north of 35°S into the STZ. These horizontal and subduction fluxes lead to small accumulations of DIC_{anth} within the mixed layer of the SAZ and the STZ, where most of the subduction occurs, while keeping the southernmost regions depleted and hence more prone to take up anthropogenic carbon (Figure S4 in Supporting Information S1).

Over 1995–2014, air-sea fluxes of anthropogenic CO_2 show a significant positive trend ($r^2 > 0.85$ and p-value < 0.05) in all regions, as expected from the increase in atmospheric pCO_2 (Figure S5a in Supporting Information S1). The highest increase occurs in the STZ and the smallest in the ASZ. Yet, no net accumulation of DIC_{anth} occurs in the mixed layer of the Southern Ocean over that period meaning that the newly absorbed anthropogenic carbon is exported out of the Southern Ocean within the mixed layer or across the mixed layer base to the ocean interior. We find that the increase in anthropogenic CO_2 uptake is almost entirely compensated by the subduction of DIC_{anth} across the mixed layer base (+0.02 PgC/year^{-2} compared to +0.015 PgC/year^{-2} for the air-sea fluxes). In our model, the subduction rate of DIC_{anth} thus adjusts to the increase in the uptake of anthropogenic CO_2 over a 20-year period, in line with Bopp et al. (2015).

In the upper 500 m, both anthropogenic and total DIC show a low bias (except for the surface total DIC), which, in turn, likely affects the advective and diffusive fluxes of carbon across the mixed layer base (Figure S4 in Supporting Information S1). Cross-frontal fluxes of anthropogenic carbon are also likely biased due to the underestimation of the anthropogenic DIC content in the SIZ and ASZ and the overestimation in the northernmost region (Figure S4d in Supporting Information S1). This latitudinal gradient in the bias of the anthropogenic DIC content could yield an overestimation of the cross-frontal fluxes.

3.2.2. Physical Drivers of Anthropogenic Carbon Transfer Across the Mixed Layer Base

When averaged over the Southern Ocean, subduction of DIC_{anth} is mainly achieved through vertical diffusion and advection, which each contribute to about half of the total flux of anthropogenic carbon toward the ocean interior (Figure 5b). While advective fluxes dominate north of the ACC, accounting for 69% of the anthropogenic DIC transferred across the mixed layer base (with respect to the sum of all in and out fluxes north of the Subantarctic Front), vertical diffusion dominates south of the Subantarctic Front, accounting for 62% of this transfer. As expected, advection brings anthropogenic carbon within the mixed layer in the southernmost regions (SIZ, ASZ) due to the large-scale upwelling of Circumpolar Deep Water, and transfers carbon into the ocean interior in the northernmost regions (SAZ, STZ) through downwelling of Antarctic Intermediate and Subantarctic Mode Waters as part of the upper cell on the Southern Ocean overturning. The SAZ and STZ host the largest subduction fluxes of anthropogenic DIC supported by advection, through the cooling and transformation of Subtropical Waters, rich in DIC_{anth}, into Subantarctic Mode Waters.

In contrast, vertical diffusion acts to transfer anthropogenic carbon below the mixed layer in all regions due to the large-scale upward vertical gradient of DIC_{anth} (Figure S4c in Supporting Information S1). The predominance of vertical diffusion south of the Polar Front arises from the strong positive gradient of DIC_{anth} across the mixed layer base, due to the presence of DIC_{anth}-depleted Circumpolar Deep Water just below the mixed layer (Figure S4c in Supporting Information S1). Seasonal entrainment acts against the vertical gradient of DIC_{anth} and brings carbon back into the mixed layer, accounting for 7% of the sum of all fluxes on a yearly average. This small net contribution, however, results from larger and both positive and negative contributions of seasonal entrainment to the transfer of carbon across the mixed layer base across seasons (Figure S8 in Supporting Information S1). Isopycnal diffusion works to transfer DIC_{anth} to the ocean interior, as a result from the vertical gradient of DIC_{anth}, and is almost negligible, representing only 5% of the total transfer over the Southern Ocean. Hence, while seasonal entrainment may be an important process at sub-seasonal scale, advection and diffusion largely dominate the transfer of DIC_{anth} across the base of the mixed layer beyond the annual scale.

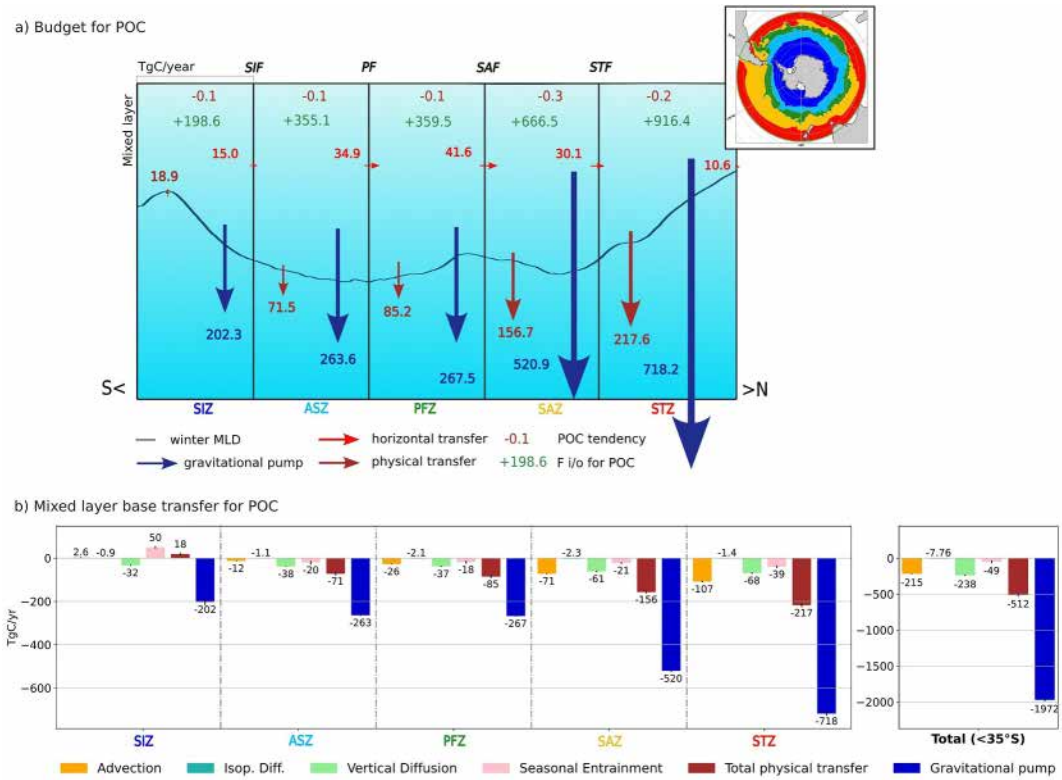

Figure 6. (a) Budget of POC in the mixed layer averaged over 1995–2014 for each of the five regions of the Southern Ocean (see definition in Section 2.3.1). The budget terms are computed following Equation 5 and expressed in TgC/year. Positive values in the mixed layer indicate a gain in POC. The physical transfer is equivalent to the ML base fluxes in Figures 4a and 5a. The insert indicates the five regions of the Southern Ocean as described in Figure 1a and Section 2.3.1. (b) Decomposition of fluxes across the base of the mixed layer for each region into the different processes following Equation 6. Positive fluxes correspond to obduction of POC within the mixed layer, and negative fluxes correspond to subduction. Error bars correspond to the interannual variability over 1995–2014. Note that the units are TgC/year in contrast to Figures 4 and 5.

3.3. Fluxes of Dissolved and Particulate Organic Carbon Within the Mixed Layer

3.3.1. Budget Within the Mixed Layer

The main source of DOC and POC to the Southern Ocean mixed layer is the transfer from the inorganic carbon pool (Figures 6a and 7a; see Section 2.3.2). In the SIZ, however, DOC mostly originates from obduction likely driven by the upwelling of Circumpolar Deep Waters, and is then transferred to the inorganic carbon pool within the mixed layer. DOC and POC production from DIC decreases with latitude, in agreement with the high Net Primary Production (NPP) occurring in the regions north of the Subantarctic Front (Figures 6a, 7a, and Figure S10 in Supporting Information S1). In all regions, POC is subducted to the ocean interior through the gravitational pump with contribution from the physical transfer except in the SIZ (Figure 6a). Similarly for DOC, the physical transfer is toward the ocean interior except in the SIZ (Figure 7a). The magnitude of the physical transfer of DOC and POC through the mixed layer base is of similar magnitude (512 TgC/year and 437 PgC/year respectively). Regionally, the physical transfer of DOC dominates that of POC south of the Subtropical Front, while the physical transfer of POC is larger than of DOC in the STZ. In total, most of the subduction of DOC and POC occurs north of the Subantarctic Front, in the SAZ and the STZ. This high transfer rate is also due to the horizontal northward transport through the fronts that bring DOC and POC to the SAZ and STZ. Yet, cross-frontal fluxes of DOC are much larger than that of POC, thus reinforcing the subduction of DOC in the northernmost regions of the Southern Ocean, while POC is largely subducted regionally, where it is created.

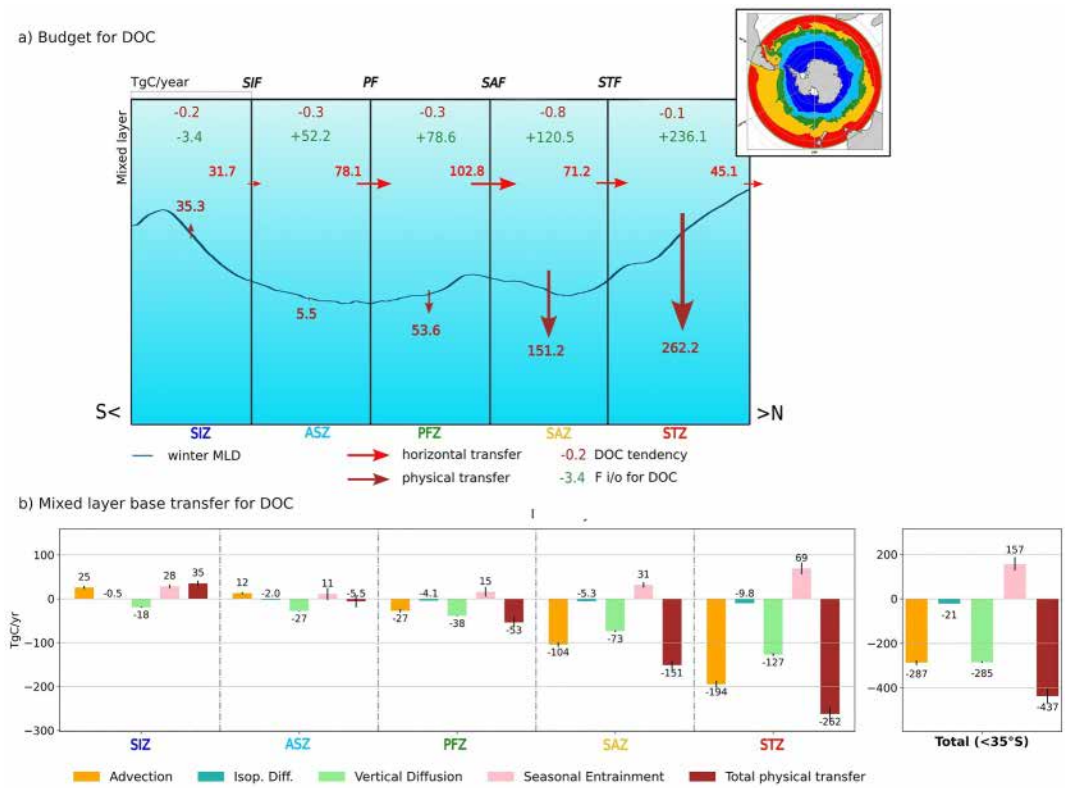

Figure 7. Same as Figure 6 but for DOC.

3.3.2. Physical Drivers of the Transfer of DOC and POC Across the Mixed Layer Base

The transfer of POC through gravitational settling (gravitational pump) is the dominant driver of the POC transfer through the base of the mixed layer (1.97 PgC/year over the Southern Ocean, Figure 6b). This transfer is twice as large as the transfer achieved through the physical transfer of DOC and POC combined. While the gravitational pump supports most of the subduction south of the Polar Front, the contribution of the physical transfer increases equatorward, reaching up to two-thirds of that of the gravitational pump in the northernmost region (STZ).

Of all the processes contributing to the physical transfer of DOC and POC across the mixed layer, vertical diffusion and advection dominate with contributions of similar sizes. However, for both DOC and POC, the contribution of vertical diffusion overtakes that of advection south of the Subantarctic Front, and reciprocally north of that front (Figures 6b and 7b). Seasonal entrainment is also a major process for DOC, counteracting vertical diffusion and advection by bringing DOC back into the mixed layer. On the contrary, seasonal entrainment is a minor process for POC subduction. The obduction of DOC in the SIZ is mostly achieved through advection (upwelling of deep waters) and seasonal entrainment in autumn and winter (Figure S9a in Supporting Information S1).

3.4. Spatial Distribution of the Fluxes Across the Mixed Layer Base

We have seen in Sections 3.1 and 3.2 that the physical transfer of the total and anthropogenic DIC across the mixed layer base is driven by advection and vertical diffusion. Locally, however, the magnitude of advective fluxes is several order of magnitude larger than that of diffusive fluxes, so that advection is the process that dominates the spatial pattern of the subduction fluxes for both total and anthropogenic DIC (Figure 8). The spatial distribution of advective fluxes is characterized by locally alternating intense obduction and subduction of DIC which, once integrated over large regions such as the interfrontal zones, cancel out to give contributions of magnitude comparable to diffusive fluxes. These alternating patterns arise from the lateral induction, that is, from the interaction between the mean flow and the sloped mixed layer base, that creates either export or import of DIC out or into the mixed layer. The contribution of the vertical advection remains generally one order of magnitude

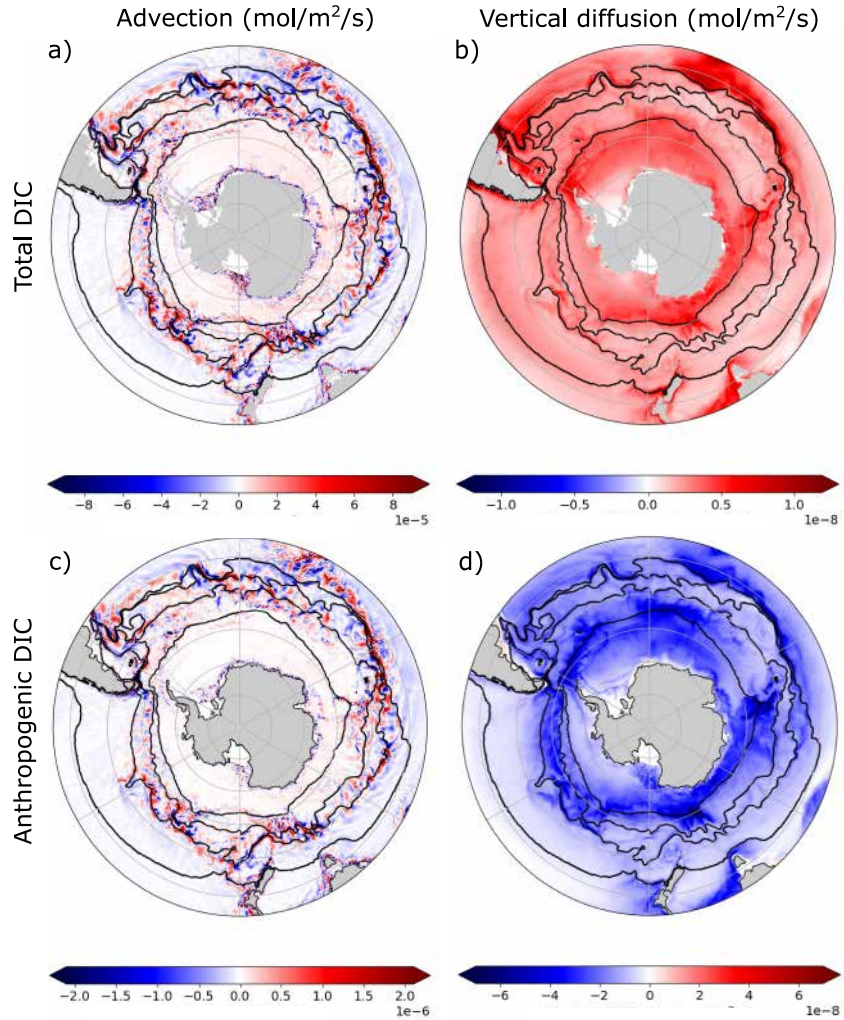

Figure 8. Maps of the two dominant processes contributing to the subduction of DIC across the mixed layer base: (a, c) advection and (b, d) vertical diffusion of (a, b) DIC_{tot} and (c, d) DIC_{anth} averaged over 1995–2014. Positive fluxes correspond to obduction. Black contours correspond to the boundaries between the five zones. Note the different scales used across the panels to help the visualization of the spatial patterns.

smaller than that of the lateral component, even over small regions (not shown). Enhanced contribution of advection can thus be found where the mixed layer base is steep and the flow is intense which is typical of western boundary currents (intense flow), and the northern ACC (PFZ and SAZ; Figure 8). Within the ACC, enhanced advective fluxes across the mixed layer base are more specifically found around major bathymetric obstacles such as the Kerguelen and Campbell Plateaus and the Drake Passage (Figure 9), that is, where the jets of the ACC accelerate and meander. As the flow circumvents these obstacles, carbon is either obducted then subducted, or the other way round, depending on the meridional gradient of the mixed layer depth. For instance, upstream of the Drake Passage, subduction occurs as the flow heads northward away from the deep mixed layers of the southeast Pacific, while downstream, obduction occurs as the flow encounters gradually deeper mixed layers (Figures 2, 8, and 9). These localized enhanced subduction fluxes downstream of topographic features, which are associated with increased mesoscale activity, are corroborated by observational evidence (Dove et al., 2021; Sallée et al., 2012) and models (also for outgassing and obduction; Youngs et al. (2023), Yung et al. (2022), Brady et al. (2021)).

The spatial patterns of the advective and diffusive transfer of DOC and POC (TOC) across the mixed layer base are generally the same as those of the DIC (Figures 10a and 10b). The gravitational pump shows an homogeneous distribution, with a strong attenuation within the SIZ, and an amplification in western boundary currents and

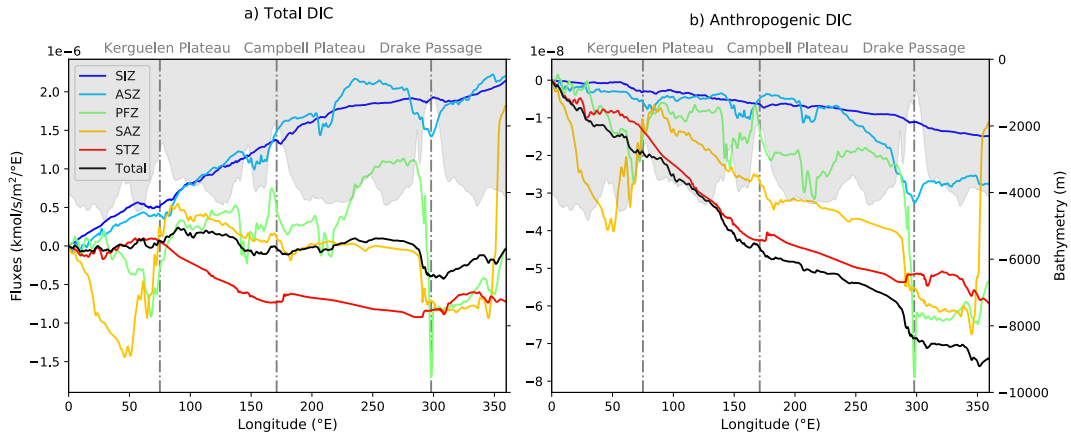

Figure 9. 1995–2014 averaged transfer of DIC across the base of the mixed layer cumulatively summed along latitude within each region (colored lines) and the Southern Ocean (black line) for (a) the total and (b) the anthropogenic inorganic carbon component. Positive values correspond to obduction. Bathymetry is shown in the background in white with the major bathymetric features indicated using vertical dashed-dotted lines.

coastal areas (in the STZ), which are regions of strong NPP (Figure 10c and Figure S10 in Supporting Information S1). The gravitational pump is found to dominate the other processes over 81% of the Southern Ocean. Yet, within frontal zones and western boundary currents, the physical transfer becomes stronger than the gravitational pump especially in the PFZ (32% of the area) and the STZ (24%).

4. Discussion

Over the Southern Ocean, the analyses of physical processes driving the transfer of DIC across the base of the mixed layer made in our model reveal that advection dominates over other processes for total DIC and contributes to half the transfer for anthropogenic DIC. The other half is attributed to the action of vertical diffusion. This result is in good agreement with recent estimates made from BGC-Argo floats measurements which show that advection is the main process driving fluxes across the mixed layer base for total DIC in the SIZ and ASZ (Sauvé et al. (2023) in their Figure 2b, our Table 2). Yet, our advective fluxes in the SIZ and the ASZ amount only to half (SIZ) or 60% (ASZ) of the advective fluxes in Sauvé et al. (2023). Besides, we find that advective fluxes are higher in the ASZ than the SIZ by 20%, when they find fluxes of equivalent sizes in both regions. Our vertical diffusion term is also almost twice as large as in their budget, however, caution should be used when comparing the magnitude of vertical diffusion with observational estimates given the heavy reliance of results on the magnitude of the diffusivity coefficients used.

Our results show an important role for advection in the transfer of DIC across the mixed layer base, in agreement with previous modeling studies. Yet, this role is found to be stronger in our model than previously shown. Using a similar model configuration as ours but at a coarser resolution (2° against 0.25°), Levy et al. (2013) found a transfer of 14.3 PgC/year of natural DIC toward the ocean interior south of 44°S, against 22.8 PgC/year in our study. The larger obduction in our model is mostly due to the advection term which is almost twice the magnitude of that found in Levy et al. (2013) (~20 PgC/year against ~12 PgC/year). As resolution is increased, a more vigorous physical circulation is resolved resulting in larger advective fluxes. Locally, these fluxes can be almost one order of magnitude larger in an eddy-permitting model than in a eddy-parameterized model (e.g., 0.25° against 2°; not shown). Yet, 0.25° resolution does not resolve the full mesoscale eddy spectrum. Processes at mesoscale and at submesoscale are known to have a non-negligible impact on tracer transport, especially at the mixed layer (Balwada et al., 2018; Calvert et al., 2020; Fox-Kemper & Ferrari, 2008). Thus, increasing the model resolution would most likely lead, at the local scale, to an increase in advective fluxes and a decrease in the diffusive fluxes (e.g., GM and Redi parameterization being muted or turned off depending on the resolution used). Yet, the net effect of refining resolution on advective fluxes of carbon is unclear, given the strong compensation of local fluxes at the larger scale as pointed out in Section 3.4. Quantifying this effect would require a dedicated study with a set of models at various resolution.

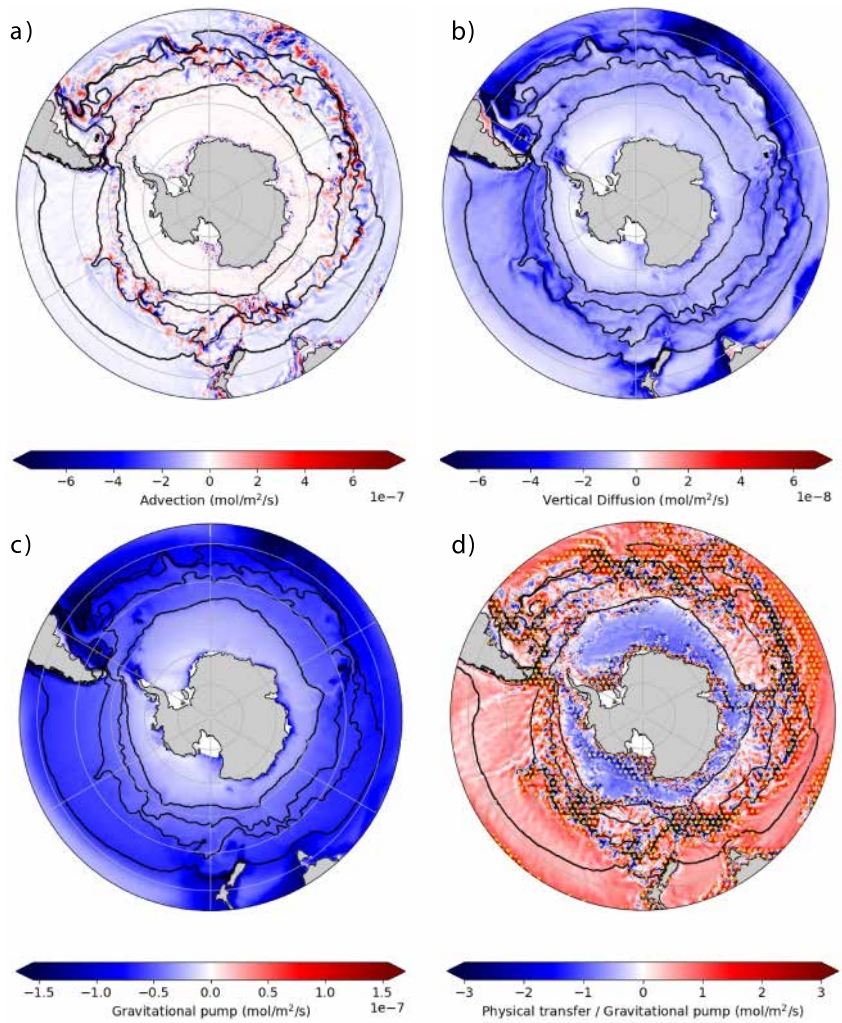

Figure 10. Maps of the three dominant processes contributing to the subduction of TOC = POC + DOC across the mixed layer base: (a) advection, (b) vertical diffusion, (c) gravitational pump. (d) Ratio between the physical transfer and the gravitational pump averaged over 1995–2014, with regions where the physical transfer is larger than the gravitational pump marked by a yellow dot pattern. Positive fluxes correspond to obduction. Black contours correspond to the boundaries between the five zones. Note the different scales used across the panels to help the visualization of the spatial patterns.

The contribution of advection is largely dependent on the region considered. For instance, when integrated south of 44°S, that is, when we move the boundary of the Southern Ocean by 9° to the south compared to our study, the contribution of vertical diffusion to the transfer of DIC_{anth} is found to largely dominate that of advection (0.42 PgC/year for vertical diffusion compared to around 0.05 PgC/year for advection). The decreased contribution from the advective term is due to the strong compensation between obduction south of the ACC and

Table 2
Comparison of Subduction Fluxes in mol/m²/year Between Our Model and the Estimates Made by Sauvé et al. (2023) for the SIZ and the ASZ Regions Based on BGC-Argo Floats

	ASZ		SIZ	
	Vertical diffusion	Advection	Vertical diffusion	Advection
Sauvé et al. (2023)	1.89	83.65	1.28	76.92
This study	2.7	50.3	3.5	40.3

Note. Estimates from Sauvé et al. (2023) are taken from their Figure 2.

subduction north of the ACC (Figure 5b). Moving the boundary of the Southern Ocean to the south thus removes the strong subduction occurring in the STZ and part of the SAZ. This predominance of vertical diffusion in transferring DIC_{ant} across the mixed layer base south of 44°S corroborates the results of Bopp et al. (2015) obtained from a configuration at 2° similar to ours and the same online diagnostics. In their study, Bopp et al. (2015) found a subduction rate by vertical mixing (combining vertical diffusion, seasonal entrainment and isopycnal diffusion) of 0.69 PgC/year for 1998–2007 (compared to 0.40 PgC/year in our study but for 1995–2014). Overall, these comparisons of fluxes across the mixed layer base integrated between different Southern Ocean domains highlight the strong dependency of flux estimates to the region studied. The five regions bounded by fronts that are used in this study thus provide a physically coherent framework to investigate the fluxes and perform inter-comparisons between models and evaluation against observations.

Within these coherent regions, fluxes across the mixed layer base show large spatial variations (Figures 8a and 8c), as described in Section 3.4. In particular, regions with powerful currents and with strong interactions between the flow and the bathymetry see carbon fluxes across the mixed layer of orders of magnitude larger than in other regions. Although similar bands can be detected in observations (Chen & Schofield, 2024; Sallée et al., 2012) and in coarser resolution models (Levy et al., 2013), their extent may not be captured or can be overestimated compared to relatively high-resolution models (this study, Brady et al. (2021) and Yung et al. (2022) for obduction fluxes). Hence, the very localized nature of these advection fluxes poses a challenge in capturing the carbon pathways between the surface and the interior from observations and coarse-resolution models.

Similarly to the inorganic carbon, the organic carbon undergoes an enhanced advective transfer across the mixed layer base, in particular within boundary currents and frontal regions (Figure 10). There, organic carbon export has been shown to be strongly associated with mesoscale and submesoscale circulations, and the mesoscale advective transport has been referred to as the eddy subduction pump (Dove et al., 2021; Lacour et al., 2023; Llort et al., 2018; Thompson et al., 2024). The eddy pump has only been observed within relatively small regions, however, so the efficiency of this pump at the basin scale remains to be quantified. Despite the incomplete resolution of mesoscale in our model, our results suggest that the eddy subduction pump may be a dominant pathway for organic carbon transfer across the mixed layer base in regions of strong mesoscale eddy activity such as the boundary currents and the fronts. Integrated over interfrontal regions, however, the contribution of the eddy subduction pump would likely be greatly reduced due to compensation between obduction and subduction. To confirm this hypothesis, a mesoscale-eddy decomposition of organic carbon fluxes would need to be performed at the mixed layer base.

In our model, the addition of the advective and isopycnal diffusive fluxes forms the eddy subduction and large scale pumps whose contributions to the organic carbon subduction are compared in the literature to the mixed layer pump, which combines the action of vertical diffusion and the seasonal entrainment (Ricour et al., 2023; D. A. Siegel et al., 2023; Thompson et al., 2024). Our analyses show that for POC, the large scale and eddy subduction pumps have a similar contribution to the mixed layer pump. For DOC, however, the large scale and eddy pump dominate together over the mixed layer pump, as vertical diffusion and seasonal entrainment tend to cancel out. When comparing the role of the physical transfer and the gravitational pump, we obtain that the physical transfer of POC represents around 26% of the gravitational pump, which is very similar to the 30% found by extrapolating observations from sediment traps (D. Siegel et al., 2008). Similar to Huang et al. (2023), we find a smaller percentage contribution of the gravitational pump in the northernmost regions of the Southern Ocean compared to the south of the ACC. However we still find a dominating role of the gravitational pump in the biological pump in the SAZ and the STZ, while it represents less than half the biological pump in Huang et al. (2023). Our model shows that the seasonal entrainment leads to an annual obduction (due to a stronger obduction in the fall than the subduction in the spring—Figure S9 in Supporting Information S1) for both POC and DOC, compensated by a stronger subduction by the vertical diffusion. Therefore, models need to include the vertical diffusion component of the mixed layer pump to compare their results to the literature on the mixed layer pump based on observations. In our analyses, the mixed layer pump contributes about as much for DOC as for POC in the Southern Ocean (128 TgC/year compared to 189 TgC/year for POC). The subduction of POC through the mixed layer pump has been shown to reach an average of 23% of the gravitational pump globally, with a larger role in the Southern Ocean due to localized deep mixed layers (Dall'Olmo et al., 2016); but the quantification of the mixed layer pump for DOC was not known, preventing a comparison with that of POC.

The role of DOC in the total transfer of organic carbon at the base of the euphotic zone was also measured to represent 20% of the total export (Huang et al., 2023; Roshan & DeVries, 2017), while in our case it represents

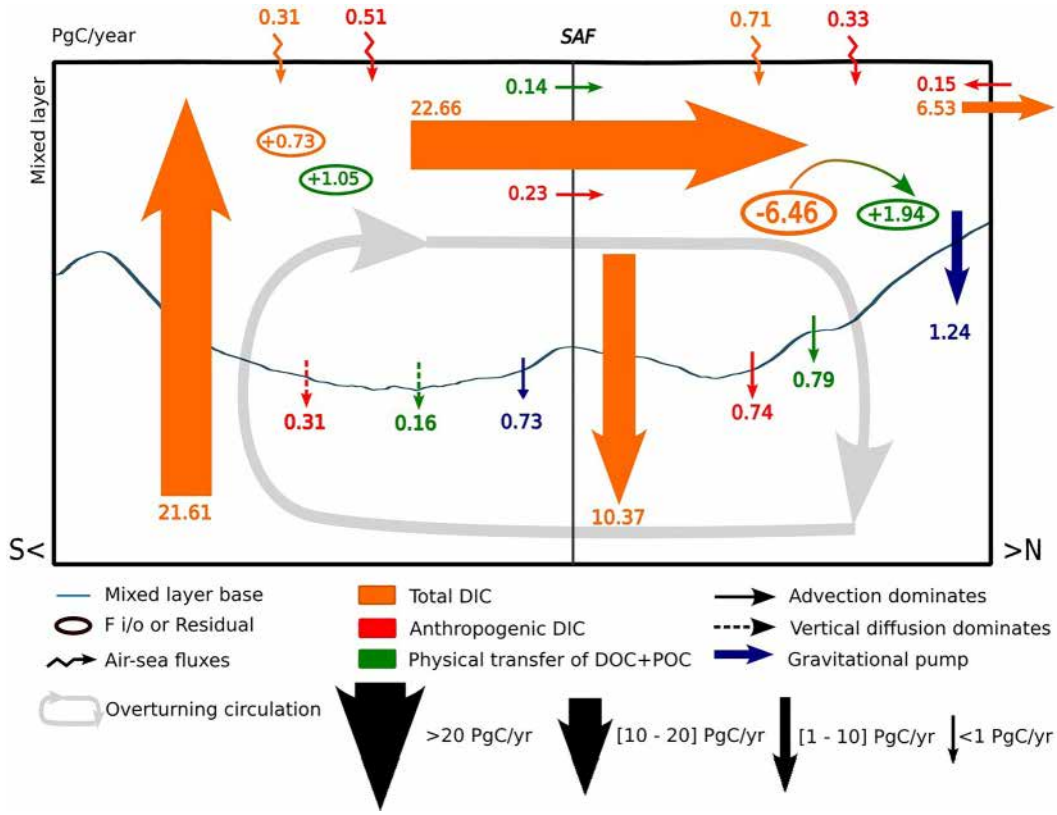

Figure 11. Schematic of the main fluxes within and across the mixed layer (straight arrows) and across the air-sea interface (wriggly arrows) for total DIC (orange), anthropogenic DIC (red), and DOC and POC (green). The size of arrows corresponds to the magnitude of the flux sorted in four size categories as indicated in the legend. Based on the results of the study, the five regions are regrouped into southern regions (SIZ, ASZ and PFZ) and northern regions (SAZ and STZ).

around 18% of all mixed layer fluxes in the Southern Ocean, all in all a very similar result. Our work confirms the conclusions from previous studies that have shown the important role of DOC in the total export of organic carbon to the ocean interior (Huang et al., 2023; Nowicki et al., 2022; Resplandy et al., 2019).

5. Conclusion

In this study, we used an eddy-permitting global ocean model to compute budgets of DIC, DOC and POC within the mixed layer of the Southern Ocean (south of 35°S) and associated fluxes across the base of the mixed layer over 1995–2014. Two simulations with the same circulation but different atmospheric CO_2 concentrations and oceanic carbon concentrations were analyzed to contrast the budget and transfer across the mixed layer of total and anthropogenic DIC, as well as DOC and POC, and to investigate the physical processes driving this transfer. Analyses are done within five physically consistent regions of the Southern Ocean providing a framework for future comparisons with observations and models. The main results are summarized in a schematic (Figure 11) and briefly listed below:

1. In the Southern Ocean, 11.24 PgC/year of total DIC is obducted into the mixed layer and 1.05 PgC/year of anthropogenic DIC is subducted into the ocean interior over 1995–2014. No net accumulation nor loss of total or anthropogenic DIC is found within the mixed layer over the 20 years investigated, the uptake of anthropogenic CO_2 being largely compensated by the subduction toward the ocean interior.
2. South of the Subantarctic Front, DIC is obducted into the mixed layer predominantly through advection and transported northward across the Subantarctic Front. North of the Subantarctic Front, DIC is subducted toward the ocean interior through advection with partial compensation by vertical diffusion. At the northern boundary of the Southern Ocean, 6.53 PgC/year of total DIC is transported to lower latitudes within the mixed layer.

Advection is the main process driving the transfer of total DIC across the base of the mixed layer in all regions, the contribution by vertical diffusion being only a third of that of advection over the Southern Ocean.

3. Anthropogenic CO_2 is taken up in similar amounts in all regions of the Southern Ocean. The anthropogenic CO_2 absorbed south of the Subantarctic Front is transferred toward the north and subducted north of the Subantarctic Front together with the anthropogenic CO_2 absorbed in this region. Advection and vertical diffusion contribute equally to the transfer of anthropogenic DIC across the mixed layer base. While vertical diffusion dominates south of the Subantarctic Front, advection is the main driver of subduction north of the Subantarctic Front.
4. The gravitational pump is the main driver of the transfer of DOC and POC through the mixed layer base, dominating over the physical transfer of both DOC and POC. The magnitude of the gravitational pump decreases with latitude, but its relative contribution to the total export increases with latitude as the physical transfer is even more reduced in these regions. Advection and vertical diffusion are equally important for the subduction of DOC and POC, advection dominating north of the Subantarctic Front, and vertical diffusion dominating south. Seasonal entrainment has a non-negligible role and obducts DOC in the SAZ and the STZ.
5. The transfer of DIC, DOC and POC across the mixed layer base via vertical diffusion is enhanced near the Sea Ice Front, and within boundary currents. Advective fluxes are intensified within the ACC fronts and the boundary currents. Importantly, these advective fluxes are very localized and strengthened near major topographic features. In these areas, the contribution of physical transfer to the subduction of POC and DOC thus dominates over the gravitational pump.

Overall, our results point to an important role of advective fluxes in transferring carbon to the ocean interior in some regions thus calling for accurate and high sampling measurements of the flow and estimates of mixed layer depth, to reconstruct carbon fluxes in these specific regions. In numerical models, vertical diffusion is still an important player in transferring carbon across the base of the mixed layer so that better representing this process requires better constraining the eddy diffusivity coefficients used in models through dedicated measurements. Our results also point toward an important role of advective fluxes for the subduction of organic carbon, which can become more important than the gravitational pump, especially in frontal regions. As the Southern Ocean represents the region of the global ocean with the largest uptake of anthropogenic carbon, a comprehensive understanding of how carbon is transported at depth in this region is critical to the projections of the future climate. This need becomes even more urgent as marine carbon dioxide removal (mCDR) approaches are beginning to be envisioned for this region. Effective monitoring, reporting, and verification of such interventions require a robust understanding of carbon transport, transformation, and exchange pathways (e.g., Boyd et al., 2025) which, given the spatio-temporal variability of carbon fluxes, will not be achieved without deploying an observational network much denser than what currently exists. Meanwhile, numerical models can be used to inform observations on where and when to sample carbon fluxes and to design experiments to probe future scenarios.

Conflict of Interest

The authors declare no conflicts of interest relevant to this study.

Data Availability Statement

The model outputs and code used in this study are available in the zenodo repository (Le Chevere et al., 2024). Global Carbon Budget fluxes can be found here at Hauck, Landschützer, et al. (2023). Observational data sets used in this study are available online, with temperature and salinity from CORA5.2 at https://data.marine.copernicus.eu/product/INSITU_GLO_PHY_TS_OA_MY_013_052/ (Szekely et al., 2019), DIC from GLODAPv2 at https://doi.org/10.3334/CDIAC/OTG.NDP093_GLODAPv2 (Lauvset et al., 2016), and MLD from http://www.jamstec.go.jp/ARGO/J_ARGOe.html (Hosoda et al., 2010). The air-sea fluxes values from Bushinsky et al. (2019) were given by the corresponding author of this article after a personal request.

Acknowledgments

SLC was supported by the Natural Sciences and Engineering Research Council of Canada (NSERC) through the Discovery Grant (RGPIN/2018-04985) awarded to C. O.D. and by the Québec Océan strategic cluster, and by the ERC-2022-STG OceanPeak (Grant 101077209), awarded to Judith Hauck, funded by the European Union. Views and opinions expressed are however those of the author(s) only and do not necessarily reflect those of the European Union or the European Research Council. Neither the European Union nor the European Research Council can be held responsible for them. The simulations used in this study were run by Christian Ethé with computational resources from Très Grand Centre de Calcul (TGCC) in the ESPRI (Ensemble de Services Pour la Recherche l'IPSL) computing and data center (https://mesocentre.ipsl.fr). SLC acknowledges financial support from Québec-Océan for this work. We thank Seth Bushinsky and Jade Sauvé for sharing their data with us. We also thank Olivier Torres and Manon Berger who helped process and transfer the model output used in this study. Finally, we thank two anonymous reviewers whose constructive comments greatly improved this manuscript.

References

Accardo, A., Laxenaire, R., Baudena, A., Speich, S., Kiko, R., & Stemmann, L. (2025). Intense and localized export of selected marine snow types at eddy edges in the South Atlantic Ocean. *Biogeosciences*, *22*(5), 1183–1201. https://doi.org/10.5194/bg-22-1183-2025

Adcroft, A., Anderson, W., Balaji, V., Blanton, C., Bushuk, M., Dufour, C. O., et al. (2019). The GFDL global ocean and sea ice model OM4.0: Model description and simulation features. *Journal of Advances in Modeling Earth Systems*, *11*(10), 3167–3211. https://doi.org/10.1029/2019MS001726

Archibald, K. M., Siegel, D. A., & Doney, S. C. (2019). Modeling the impact of zooplankton diel vertical migration on the carbon export flux of the biological pump. *Global Biogeochemical Cycles*, *33*(2), 181–199. https://doi.org/10.1029/2018GB005983

Aumont, O., Ethé, C., Tagliabue, A., Bopp, L., & Gehlen, M. (2015). PISCES-v2: An ocean biogeochemical model for carbon and ecosystem studies. *Geoscientific Model Development*, *8*(8), 2465–2513. https://doi.org/10.5194/gmd-8-2465-2015

Baker, K., Halfter, S., Scoulding, B., Swadling, K. M., Richards, S. A., Bressac, M., et al. (2025). Carbon injection potential of the mesopelagic-migrant pump in the Southern Ocean during summer. *Frontiers in Marine Science*, *12*, 1461723. https://doi.org/10.3389/fmars.2025.1461723

Bakker, D. C. E., Pfeil, B., Landa, C. S., Metzl, N., O'Brien, K. M., Olsen, A., et al. (2016). A multi-decade record of high-quality CO2 data in version 3 of the surface ocean CO2 Atlas (SOCAT). *Earth System Science Data*, *8*(2), 383–413. https://doi.org/10.5194/essd-8-383-2016

Balwada, D., Smith, K. S., & Abernathey, R. (2018). Submesoscale vertical velocities enhance tracer subduction in an idealized antarctic circumpolar current. *Geophysical Research Letters*, *45*(18), 9790–9802. https://doi.org/10.1029/2018GL079244

Blanke, B., & Delecluse, P. (1993). Variability of the tropical Atlantic Ocean simulated by a general circulation model with two different mixed-layer physics. *Journal of Physical Oceanography*, *23*(7), 1363–1388. https://doi.org/10.1175/1520-0485(1993)023<1363:VOTTAO>2.0.CO;2

Bopp, L., Lévy, M., Resplandy, L., & Sallée, J. B. (2015). Pathways of anthropogenic carbon subduction in the global ocean. *Geophysical Research Letters*, *42*(15), 6416–6423. https://doi.org/10.1002/2015GL065073

Boyd, P. W., Claustre, H., Levy, M., Siegel, D. A., & Weber, T. (2019). Multi-faceted particle pumps drive carbon sequestration in the ocean. *Nature*, *568*(7752), 327–335. https://doi.org/10.1038/s41586-019-1098-2

Boyd, P. W., Gattuso, J.-P., Legendre, L., Moustakis, Y., & Pongratz, J. (2025). Effective carbon dioxide removal requires a One-Earth approach. *Environmental Research Letters*, *20*(11), 111004. https://doi.org/10.1088/1748-9326/ae15a8

Brady, R. X., Maltrud, M. E., Wolfram, P. J., Drake, H. F., & Lovenduski, N. S. (2021). The influence of ocean topography on the upwelling of carbon in the Southern Ocean. *Geophysical Research Letters*, *48*(19), e2021GL095088. https://doi.org/10.1029/2021GL095088

Bushinsky, S. M., Landschützer, P., Rödenbeck, C., Gray, A. R., Baker, D., Mazloff, M. R., et al. (2019). Reassessing Southern Ocean air-sea CO_2 flux estimates with the addition of biogeochemical float observations. *Global Biogeochemical Cycles*, *33*(11), 1370–1388. https://doi.org/10.1029/2019GB006176

Calvert, D., Nurser, G., Bell, M. J., & Fox-Kemper, B. (2020). The impact of a parameterisation of submesoscale mixed layer eddies on mixed layer depths in the NEMO ocean model. *Ocean Modelling*, *154*, 101678. https://doi.org/10.1016/j.ocemod.2020.101678

Carroll, D., Menemenlis, D., Dutkiewicz, S., Lauderdale, J. M., Adkins, J. F., Bowman, K. W., et al. (2022). Attribution of space-time variability in global-ocean dissolved inorganic carbon. *Global Biogeochemical Cycles*, *36*(3), e2021GB007162. https://doi.org/10.1029/2021GB007162

Chen, M. L., & Schofield, O. (2024). Spatial and seasonal controls on eddy subduction in the Southern Ocean. *Geophysical Research Letters*, *51*(20), e2024GL109246. https://doi.org/10.1029/2024GL109246

Dall'Olmo, G., Dingle, J., Polimene, L., Brewin, R. J. W., & Claustre, H. (2016). Substantial energy input to the mesopelagic ecosystem from the seasonal mixed-layer pump. *Nature Geoscience*, *9*(11), 820–823. https://doi.org/10.1038/ngeo2818

Davila, X., Gebbie, G., Brakstad, A., Lauvset, S. K., McDonagh, E. L., Schwinger, J., & Olsen, A. (2022). How is the ocean anthropogenic carbon reservoir filled? *Global Biogeochemical Cycles*, *36*(5), e2021GB007055. https://doi.org/10.1029/2021GB007055

de Boyer Montégut, C. (2004). Mixed layer depth over the global ocean: An examination of profile data and a profile-based climatology. *Journal of Geophysical Research*, *109*(C12), C12003. https://doi.org/10.1029/2004JC002378

DeVries, T. (2014). The oceanic anthropogenic CO_2 sink: Storage, air-sea fluxes, and transports over the industrial era. *Global Biogeochemical Cycles*, *28*(7), 631–647. https://doi.org/10.1002/2013GB004739

DeVries, T., Holzer, M., & Primeau, F. (2017). Recent increase in oceanic carbon uptake driven by weaker upper-ocean overturning. *Nature*, *542*(7640), 215–218. https://doi.org/10.1038/nature21068

Dove, L. A., Thompson, A. F., Balwada, D., & Gray, A. R. (2021). Observational evidence of ventilation hotspots in the Southern Ocean. *Journal of Geophysical Research: Oceans*, *126*(7), e2021JC017178. https://doi.org/10.1029/2021JC017178

Dufour, C. O., Griffies, S. M., de Souza, G. F., Frenger, I., Morrison, A. K., Palter, J. B., et al. (2015). Role of mesoscale eddies in cross-frontal transport of heat and biogeochemical tracers in the Southern Ocean. *Journal of Physical Oceanography*, *45*(12), 3057–3081. https://doi.org/10.1175/JPO-D-14-0240.1

Dufour, C. O., Sommer, J. L., Gehlen, M., Orr, J. C., Molines, J., Simeon, J., & Barnier, B. (2013). Eddy compensation and controls of the enhanced sea-to-air CO_2 flux during positive phases of the Southern Annular Mode. *Global Biogeochemical Cycles*, *27*(3), 950–961. https://doi.org/10.1002/gbc.20090

Dussin, R., Barnier, B., Brodeau, L., & Molines, J.-M. (2016). The making of the DRAKKAR FORCING SET DFS5. DRAKKAR/MyOcean Report.

Fox-Kemper, B., & Ferrari, R. (2008). Parameterization of mixed layer eddies. Part II: Prognosis and impact. *Journal of Physical Oceanography*, *38*(6), 1166–1179. https://doi.org/10.1175/2007JPO3788

Friedlingstein, P., O'Sullivan, M., Jones, M. W., Andrew, R. M., Hauck, J., Olsen, A., et al. (2020). Global Carbon Budget 2020. *Earth System Science Data*, *12*(4), 3269–3340. https://doi.org/10.5194/essd-12-3269-2020

Frölicher, T. L., Sarmiento, J. L., Paynter, D. J., Dunne, J. P., Krasting, J. P., & Winton, M. (2015). Dominance of the Southern Ocean in anthropogenic carbon and heat uptake in CMIP5 models. *Journal of Climate*, *28*(2), 862–886. https://doi.org/10.1175/JCLI-D-14-00117.1

Gent, P., & McWilliams, J. (1990). Isopycnal mixing in ocean circulation models. *Journal of Physical Oceanography*, *20*, 150–155. https://doi.org/10.1175/1520-0485(1990)020⟨0150:IMIOCM⟩2.0.CO;2

Gent, P., McWilliams, J., Willebrand, J., & McDougall, T. J. (1995). Parameterizing eddy-induced tracer transports in ocean circulation models. *Journal of Physical Oceanography*, *25*(4), 463–474. https://doi.org/10.1175/1520-0485(1995)025<0463:peitti>2.0.co;2

Giering, S., Sanders, R., Blackbird, S., Briggs, N., Carvalho, F., East, H., et al. (2023). Vertical imbalance in organic carbon budgets is indicative of a missing vertical transfer during a phytoplankton bloom near South Georgia (COMICS). *Deep Sea Research Part II: Topical Studies in Oceanography*, *209*, 105277. https://doi.org/10.1016/j.dsr2.2023.105277

Graven, H. D., Gruber, N., Key, R., Khatiwala, S., & Giraud, X. (2012). Changing controls on oceanic radiocarbon: New insights on shallow-to-deep ocean exchange and anthropogenic CO_2 uptake: Changing controls on oceanic ^{14}C. *Journal of Geophysical Research*, *117*(C10). https://doi.org/10.1029/2012JC008074

Gray, A. R., Johnson, K. S., Bushinsky, S. M., Riser, S. C., Russell, J. L., Talley, L. D., et al. (2018). Autonomous biogeochemical floats detect significant carbon dioxide outgassing in the high-latitude Southern Ocean. *Geophysical Research Letters*, *45*(17), 9049–9057. https://doi.org/10.1029/2018GL078013

Gruber, N., Landschützer, P., & Lovenduski, N. S. (2019). The variable Southern Ocean carbon sink. *Annual Review of Marine Science*, *11*(1), 159–186. https://doi.org/10.1146/annurev-marine-121916-063407

Hallberg, R. (2013). Using a resolution function to regulate parameterizations of oceanic mesoscale eddy effects. *Ocean Modelling*, *72*, 92–103. https://doi.org/10.1016/j.ocemod.2013.08.007

Hansell, D. A. (2013). Recalcitrant dissolved organic carbon fractions. *Annual Review of Marine Science*, *5*(1), 421–445. https://doi.org/10.1146/annurev-marine-120710-100757

Hauck, J., Gregor, L., Nissen, C., Patara, L., Hague, M., Mongwe, P., et al. (2023). The Southern Ocean carbon cycle 1985–2018: Mean, seasonal cycle, trends, and storage. *Global Biogeochemical Cycles*, *37*(11), e2023GB007848. https://doi.org/10.1029/2023GB007848

Hauck, J., Landschützer, P., Mayot, N., & Jersild, A. (2023). Global Carbon Budget 2023, surface ocean fugactiy of CO2 (fCO2) and air-sea CO2 flux of individual global ocean biogechemical models and surface ocean fCO2-based data-products. *Zenodo*. https://doi.org/10.5281/ZENODO.10222483

Hauck, J., Zeising, M., Le Quéré, C., Gruber, N., Bakker, D. C. E., Bopp, L., et al. (2020). Consistency and challenges in the Ocean carbon sink estimate for the global carbon budget. *Frontiers in Marine Science*, *7*, 571720. https://doi.org/10.3389/fmars.2020.571720

Hosoda, S., Ohira, T., Sato, K., & Suga, T. (2010). Improved description of global mixed-layer depth using Argo profiling floats. *Journal of Oceanography*, *66*(6), 773–787. https://doi.org/10.1007/s10872-010-0063-3

Huang, Y., Fassbender, A., & Bushinsky, S. (2023). Biogenic carbon pool production maintains the Southern Ocean carbon sink. *Proceedings of the National Academy of Sciences*, *120*(18), e2217909120. https://doi.org/10.1073/pnas.2217909120

Iudicone, D., Rodgers, K. B., Stendardo, I., Aumont, O., Madec, G., Bopp, L., et al. (2011). Water masses as a unifying framework for understanding the Southern Ocean Carbon Cycle. *Biogeosciences*, *8*(5), 1031–1052. https://doi.org/10.5194/bg-8-1031-2011

Karleskind, P., Lévy, M., & Memery, L. (2011). Subduction of carbon, nitrogen, and oxygen in the northeast Atlantic. *Journal of Geophysical Research*, *116*(C2), C02025. https://doi.org/10.1029/2010JC006446

Lacour, L., Llort, J., Briggs, N., Strutton, P. G., & Boyd, P. W. (2023). Seasonality of downward carbon export in the Pacific Southern Ocean revealed by multi-year robotic observations. *Nature Communications*, *14*(1), 1278. https://doi.org/10.1038/s41467-023-36954-7

Landschützer, P., Gruber, N., & Bakker, D. C. E. (2016). Decadal variations and trends of the global ocean carbon sink. *Global Biogeochemical Cycles*, *30*(10), 1396–1417. https://doi.org/10.1002/2015GB005359

Landschützer, P., Laruelle, G. G., Roobaert, A., & Regnier, P. (2020). A uniform pCO_2 climatology combining open and coastal oceans. *Earth System Science Data*, *12*(4), 2537–2553. https://doi.org/10.5194/essd-12-2537-2020

Lauvset, S. K., Key, R. M., Olsen, A., van Heuven, S., Velo, A., Lin, X., et al. (2016). A new global interior ocean mapped climatology: The 1°×1° GLODAP version 2. *Earth System Science Data*, *8*(2), 325–340. https://doi.org/10.5194/essd-8-325-2016

Le Chevere, S., Dufour, C. O., Laurent, B., & Lévy, M. (2024). Physical processes driving carbon subduction in the Southern Ocean in an eddy-permitting model [Dataset]. *Zenodo*. https://doi.org/10.5281/zenodo.14057544

Levy, M., Bopp, L., Karleskind, P., Resplandy, L., Ethe, C., & Pinsard, F. (2013). Physical pathways for carbon transfers between the surface mixed layer and the ocean interior. *Global Biogeochemical Cycles*, *27*(4), 1001–1012. https://doi.org/10.1002/gbc.20092

Li, Z., England, M. H., Groeskamp, S., Cerovečki, I., & Luo, Y. (2021). The origin and fate of subantarctic mode water in the Southern Ocean. *Journal of Physical Oceanography*. https://doi.org/10.1175/JPO-D-20-0174.1

Llort, J., Langlais, C., Matear, R., Moreau, S., Lenton, A., & Strutton, P. G. (2018). Evaluating Southern Ocean carbon eddy-pump from biogeochemical-argo floats. *Journal of Geophysical Research: Oceans*, *123*(2), 971–984. https://doi.org/10.1002/2017JC012861

Lumpkin, R., & Speer, K. (2007). Global Ocean meridional overturning. *Journal of Physical Oceanography*, *37*(10), 2550–2562. https://doi.org/10.1175/JPO3130.1

Madec, G. (2008). *NEMO ocean engine*. Institut Pierre-Simon Laplace (IPSL). https://doi.org/10.5281/zenodo.3878122

Madec, G., & the NEMO Team. (2016). NEMO ocean engine - Note du Pôle de modélisation de l'Institut Pierre-Simon Laplace No 27. Retrieved from https://www.nemo-ocean.eu/doc/

Madec, G., Delécluse, P., Imbard, M., & Lévy, C. (1998). OPA 8.1 Ocean General Circulation Model reference manual. *Notes du pôle de modelisation, laboratoire d'océanographie dynamique et de climatologie, Institut Pierre Simon Laplace des sciences de l'environnement global*, *11*.

Marshall, J., & Speer, K. (2012). Closure of the meridional overturning circulation through Southern Ocean upwelling. *Nature Geoscience*, *5*(3), 171–180. https://doi.org/10.1038/ngeo1391

Mathiot, P., Jenkins, A., Harris, C., & Madec, G. (2017). Explicit representation and parametrised impacts of under ice shelf seas in the z* coordinate ocean model NEMO 3.6. *Geoscientific Model Development*, *10*(7), 2849–2874. https://doi.org/10.5194/gmd-10-2849-2017

Maurer, T. L., Plant, J. N., & Johnson, K. S. (2021). Delayed-mode quality control of oxygen, nitrate and pH data on SOCCOM biogeochemical profiling floats (preprint). *Oceanography*. https://doi.org/10.1002/essoar.10506241.1

Mikaloff Fletcher, S. E., Gruber, N., Jacobson, A. R., Doney, S. C., Dutkiewicz, S., Gerber, M., et al. (2006). Inverse estimates of anthropogenic CO_2 uptake, transport, and storage by the ocean. *Global Biogeochemical Cycles*, *20*(2). https://doi.org/10.1029/2005GB002530

Mikaloff Fletcher, S. E., Gruber, N., Jacobson, A. R., Gloor, M., Doney, S. C., Dutkiewicz, S., et al. (2007). Inverse estimates of the oceanic sources and sinks of natural CO_2 and the implied oceanic carbon transport. *Global Biogeochemical Cycles*, *21*(1). https://doi.org/10.1029/2006GB002751

Nowicki, M., DeVries, T., & Siegel, D. A. (2022). Quantifying the carbon export and sequestration pathways of the ocean's biological carbon pump. *Global Biogeochemical Cycles*, *36*(3), e2021GB007083. https://doi.org/10.1029/2021GB007083

Olsen, A., Key, R. M., van Heuven, S., Lauvset, S. K., Velo, A., Lin, X., et al. (2016). The Global Ocean Data Analysis Project version 2 (GLODAPv2) – An internallyconsistent data product for the world ocean. *Earth System Science Data*, *8*(2), 297–323. https://doi.org/10.5194/essd-8-297-2016

Orr, J. C., Maier-Reimer, E., Mikolajewicz, U., Monfray, P., Sarmiento, J. L., Toggweiler, J. R., et al. (2001). Estimates of anthropogenic carbon uptake from four three-dimensional global ocean models. *Global Biogeochemical Cycles*, *15*(1), 43–60. https://doi.org/10.1029/2000GB001273

Orr, J. C., Najjar, R. G., Aumont, O., Bopp, L., Bullister, J. L., Danabasoglu, G., et al. (2017). Biogeochemical protocols and diagnostics for the CMIP6 Ocean Model Intercomparison Project (OMIP). *Geoscientific Model Development*, *10*(6), 2169–2199. https://doi.org/10.5194/gmd-10-2169-2017

Orsi, A. H., Whitworth, T., & Nowlin, W. D. (1995). On the meridional extent and fronts of the Antarctic Circumpolar Current. *Deep Sea Research Part I: Oceanographic Research Papers*, *42*(5), 641–673. https://doi.org/10.1016/0967-0637(95)00021-W

Park, Y.-H., Charriaud, E., & Fieux, M. (1998). Thermohaline structure of the Antarctic surface water/winter water in the Indian sector of the Southern Ocean. *Journal of Marine Systems*, *17*(1–4), 5–23. https://doi.org/10.1016/S0924-7963(98)00026-8

Redi, M. H. (1982). Oceanic isopycnal mixing by coordinate rotation. *Journal of Physical Oceanography*, *12*(10), 1154–1158. https://doi.org/10.1175/1520-0485(1982)012<1154:oimbcr>2.0.co;2

Resplandy, L., Lévy, M., & McGillicuddy, D. J. (2019). Effects of eddy-driven subduction on ocean biological carbon pump. *Global Biogeochemical Cycles*, *33*(8), 1071–1084. https://doi.org/10.1029/2018GB006125

Ricour, F., Guidi, L., Gehlen, M., DeVries, T., & Legendre, L. (2023). Century-scale carbon sequestration flux throughout the ocean by the biological pump. *Nature Geoscience*, *16*(12), 1105–1113. https://doi.org/10.1038/s41561-023-01318-9

Rodgers, K. B., Aumont, O., Mikaloff Fletcher, S. E., Plancherel, Y., Bopp, L., De Boyer Montégut, C., et al. (2014). Strong sensitivity of Southern Ocean carbon uptake and nutrient cycling to wind stirring. *Biogeosciences*, *11*(15), 4077–4098. https://doi.org/10.5194/bg-11-4077-2014

Roshan, S., & DeVries, T. (2017). Efficient dissolved organic carbon production and export in the oligotrophic ocean. *Nature Communications*, *8*(1), 2036. https://doi.org/10.1038/s41467-017-02227-3

Sabine, C. L., Feely, R. A., Gruber, N., Key, R. M., Lee, K., Bullister, J. L., et al. (2004). The oceanic sink for anthropogenic CO2. *Science*, *305*(5682), 367–371. https://doi.org/10.1126/science.1097403

Sallée, J.-B., Matear, R. J., Rintoul, S. R., & Lenton, A. (2012). Localized subduction of anthropogenic carbon dioxide in the Southern Hemisphere oceans. *Nature Geoscience*, *5*(8), 579–584. https://doi.org/10.1038/ngeo1523

Sarmiento, J. L., Orr, J. C., & Siegenthaler, U. (1992). A perturbation simulation of CO_2 uptake in an ocean general circulation model. *Journal of Geophysical Research*, *97*(C3), 3621–3645. https://doi.org/10.1029/91JC02849

Sauvé, J., Gray, A. R., Prend, C. J., Bushinsky, S. M., & Riser, S. C. (2023). Carbon outgassing in the Antarctic Circumpolar Current is supported by Ekman transport from the sea ice zone in an observation-based seasonal mixed-layer budget. *Journal of Geophysical Research: Oceans*, *128*(11), e2023JC019815. https://doi.org/10.1029/2023JC019815

Schlitzer, R. (2002). Carbon export fluxes in the Southern Ocean: Results from inverse modeling and comparison with satellite-based estimates. *Deep Sea Research Part II: Topical Studies in Oceanography*, *49*(9–10), 1623–1644. https://doi.org/10.1016/S0967-0645(02)00004-8

Siegel, D., Fields, E., & Buesseler, K. (2008). A bottom-up view of the biological pump: Modeling source funnels above ocean sediment traps. *Deep Sea Research Part I: Oceanographic Research Papers*, *55*(1), 108–127. https://doi.org/10.1016/j.dsr.2007.10.006

Siegel, D. A., DeVries, T., Cetinić, I., & Bisson, K. M. (2023). Quantifying the ocean's biological pump and its carbon cycle impacts on global scales. *Annual Review of Marine Science*, *15*(1), 329–356. https://doi.org/10.1146/annurev-marine-040722-115226

Stukel, M. R., & Ducklow, H. W. (2017). Stirring up the biological pump: Vertical mixing and carbon export in the Southern Ocean: Vertical mixing and carbon export in SO. *Global Biogeochemical Cycles*, *31*(9), 1420–1434. https://doi.org/10.1002/2017GB005652

Styles, A. F., MacGilchrist, G. A., Bell, M. J., & Marshall, D. P. (2024). Spatial and temporal patterns of Southern Ocean ventilation. *Geophysical Research Letters*, *51*(4), e2023GL106716. https://doi.org/10.1029/2023GL106716

Szekely, T., Gourrion, J., Pouliquen, S., & Reverdin, G. (2019). The CORA 5.2 dataset for global in situ temperature and salinity measurements: Data description and validation. *Ocean Science*, *15*(6), 1601–1614. https://doi.org/10.5194/os-15-1601-2019

Talley, L. D. (2013). Closure of the global overturning circulation through the Indian, Pacific, and Southern Oceans: Schematics and transports. *Oceanography*, *26*(1), 80–97. https://doi.org/10.5670/oceanog.2013.07

Terhaar, J., Orr, J. C., Gehlen, M., Ethé, C., & Bopp, L. (2019). Model constraints on the anthropogenic carbon budget of the Arctic Ocean. *Biogeosciences*, *16*(11), 2343–2367. https://doi.org/10.5194/bg-16-2343-2019

Thompson, A. F., Dove, L. A., Flint, E., Lacour, L., & Boyd, P. (2024). Interactions between multiple physical particle injection pumps in the Southern Ocean. *Global Biogeochemical Cycles*, *38*(12), e2024GB008122. https://doi.org/10.1029/2024GB008122

Toyama, K., Rodgers, K. B., Blanke, B., Iudicone, D., Ishii, M., Aumont, O., & Sarmiento, J. L. (2017). Large reemergence of anthropogenic carbon into the ocean's surface mixed layer sustained by the ocean's overturning circulation. *Journal of Climate*, *30*(21), 8615–8631. https://doi.org/10.1175/JCLI-D-16-0725.1

Vancoppenolle, M., Fichefet, T., & Goosse, H. (2009). Simulating the mass balance and salinity of Arctic and Antarctic sea ice. 2. Importance of sea ice salinity variations. *Ocean Modelling*, *27*(1–2), 54–69. https://doi.org/10.1016/j.ocemod.2008.11.003

Wanninkhof, R. (1992). Relationship between wind speed and gas exchange over the ocean. *Journal of Geophysical Research*, *97*(C5), 7373–7382. https://doi.org/10.1029/92JC00188

Williams, N. L., Juranek, L. W., Feely, R. A., Johnson, K. S., Sarmiento, J. L., Talley, L. D., et al. (2017). Calculating surface ocean pCO_2 from biogeochemical Argo floats equipped with pH: An uncertainty analysis: Calculating Ocean pCO_2 from Float pH. *Global Biogeochemical Cycles*, *31*(3), 591–604. https://doi.org/10.1002/2016GB005541

Youngs, M. K., Freilich, M. A., & Lovenduski, N. S. (2023). Air-Sea CO_2 fluxes localized by topography in a Southern Ocean channel. *Geophysical Research Letters*, *50*(18), e2023GL104802. https://doi.org/10.1029/2023GL104802

Yung, C. K., Morrison, A. K., & Hogg, A. M. (2022). Topographic hotspots of Southern Ocean Eddy upwelling. *Frontiers in Marine Science*, *9*, 855785. https://doi.org/10.3389/fmars.2022.855785